Journal of Computational Physics 366 (2018) 252–280

Contents lists available at ScienceDirect

Journal of Computational Physics

www.elsevier.com/locate/jcp

Multi-dimensional shear shallow water flows: Problems and solutions

S. Gavrilyuk [a,b,*], K. Ivanova [a], N. Favrie [a]

[a] Aix-Marseille Université, CNRS, IUSTI, UMR 7343, 5 rue E. Fermi, 13453 Marseille Cedex 13, France
[b] Novosibirsk State University, 2 Pirogova street, 630090 Novosibirsk, Russia

ARTICLE INFO

Article history:
Received 29 May 2017
Received in revised form 2 April 2018
Accepted 5 April 2018
Available online 10 April 2018

Keywords:
Non-conservative hyperbolic equations
Godunov-type methods
Roll waves

ABSTRACT

The mathematical model of shear shallow water flows of constant density is studied. This is a $2D$ hyperbolic non-conservative system of equations that is mathematically equivalent to the Reynolds-averaged model of barotropic turbulent flows. The model has three families of characteristics corresponding to the propagation of surface waves, shear waves and average flow (contact characteristics). The system is non-conservative: for six unknowns (the fluid depth, two components of the depth averaged horizontal velocity, and three independent components of the symmetric Reynolds stress tensor) one has only five conservation laws (conservation of mass, momentum, energy and mathematical 'entropy'). A splitting procedure for solving such a system is proposed allowing us to define a weak solution. Each split subsystem contains only one family of waves (either surface or shear waves) and contact characteristics. The accuracy of such an approach is tested on $2D$ analytical solutions describing the flow with linear with respect to the space variables velocity, and on the solutions describing $1D$ roll waves. The capacity of the model to describe the full transition scenario as commonly seen in the formation of roll waves: from uniform flow to $1D$ roll waves, and, finally, to $2D$ transverse 'fingering' of the wave profiles, is shown.

1. Introduction

The Saint-Venant equations (conventional shallow water equations) [5] are of great importance both in hydraulic and oceanographic applications. The reason is that they are simpler compared to the n-dimensional Euler equations with a free surface. Indeed, the Saint-Venant equations describe the evolution of the fluid depth and depth averaged velocities defined in a fixed $n-1$ dimensional domain. They form a hyperbolic system of equations in conservative form for which classical numerical methods can be applied [24,29,50]. The derivation of Saint-Venant equations is based on the smallness of the parameter $\varepsilon = H/L$ where H and L are the vertical and horizontal scale lengths, respectively, and the hypothesis that the dependence of the horizontal velocity on the vertical coordinate is very weak, i.e. the fluid flow is almost potential (the flow is not sheared). Since the shear effects are completely neglected in the model derivation, the Saint-Venant equations are not able to describe neither the formation of large scale eddies ('roller') appearing in the hydraulic jumps near the free surface nor the form of the hydraulic jump. A natural extension of the Saint-Venant equations are integro-differential Benney's equations [7] describing shear shallow water flows of uniform density. The notion of hyperbolicity of the Benney equations was introduced in [46,47,30,9]. Benney's equations admit, in particular, a linear vertical shear with constant vorticity as an

* Corresponding author at: Aix-Marseille Université, CNRS, IUSTI, UMR 7343, 5 rue E. Fermi, 13453 Marseille Cedex 13, France.
E-mail addresses: sergey.gavrilyuk@univ-amu.fr (S. Gavrilyuk), ivanova.kseniya15@gmail.com (K. Ivanova), nicolas.favrie@univ-amu.fr (N. Favrie).

https://doi.org/10.1016/j.jcp.2018.04.011
0021-9991/

exact solution. A numerical approach based on such a linear approximation was developed in [48] in $1D$ case. To the best of our knowledge, $2D$ computations of the Benney equations are absent in the literature.

For shear flows with varying in space and time vorticity an intermediate model was recently proposed where the governing equations are obtained by depth averaging of Euler equations without assuming potential flow [49,38–40]. The hypothesis of smallness of the horizontal vorticity (the hypothesis of weakly sheared flows) allows us to keep the second order depth averaged correlations in the governing equations but neglect the third order correlations, and thus to close the governing system. This approach was further extended to the case where the third-order correlations are taken into account [14].

This intermediate multi-dimensional model is reminiscent of the classical Reynolds averaged Euler equations for the compressible barotropic turbulent flows [22]. The model complemented by friction terms was used for the study of $1D$ travelling waves down inclined plane (roll waves) and hydraulic jumps. A strong physical adequacy of the model with the experimental observations was found [38–40].

The multi-dimensional case is much more challenging. For the flows over a flat bottom without friction effects, the system can be written in the form [49,40,21]:

$$\begin{aligned} &h_t + \operatorname{div}(h\mathbf{u}) = 0, \\ &(h\mathbf{u})_t + \operatorname{div}\left(h\mathbf{u}\otimes\mathbf{u} + \frac{gh^2}{2}\mathbf{I} + h\mathbf{P}\right) = \mathbf{0}, \\ &\frac{D\mathbf{P}}{Dt} + \frac{\partial \mathbf{u}}{\partial \mathbf{x}}\mathbf{P} + \mathbf{P}\left(\frac{\partial \mathbf{u}}{\partial \mathbf{x}}\right)^T = 0, \ \frac{D}{Dt} = \frac{\partial}{\partial t} + \mathbf{u}\cdot\nabla. \end{aligned} \tag{1}$$

Here t is the time, $\mathbf{x} = (x, y)^T$ are the Cartesian coordinates, $\mathbf{u} = (u, v)^T$ is the depth averaged horizontal velocity, h is the fluid depth, g is the gravity, and $\mathbf{P}$ is the stress tensor which measures the distortion of the instantaneous horizontal velocity profile $\tilde{\mathbf{u}}(t, x, y, z)$ depending of the vertical coordinate z. The sign $\otimes$ means the tensor product, and $\mathbf{I}$ is the identity tensor. The definitions of $\mathbf{u}(t, x)$ and $\mathbf{P}$ are as follows:

$$\mathbf{u}(t,x) = \frac{1}{h}\int_0^h \tilde{\mathbf{u}}(t,x,y,z)dz, \ \mathbf{P} = \frac{1}{h}\int_0^h \left(\tilde{\mathbf{u}} - \mathbf{u}\right)\otimes\left(\tilde{\mathbf{u}} - \mathbf{u}\right)dz.$$

The tensor $\mathbf{P}$ is symmetric and positive definite. The positive definiteness of $\mathbf{P}$ is a consequence of the Cauchy–Schwarz inequality.

A striking mathematical analogy with the Reynolds averaging equations of barotropic compressible turbulent flows [32,53,55,21] allows us to call $\mathbf{R} = h\mathbf{P}$ the Reynolds stress tensor, and $\mathbf{P}$ the reduced Reynolds stress tensor. For mathematical reasons, the choice of $\mathbf{P}$ is more convenient than that of $\mathbf{R}$. For simplicity, both $\mathbf{R}$ and $\mathbf{P}$ will be further refereed to as the Reynolds stress tensor.[1]

Equations (1) admit the energy conservation law:

$$\frac{\partial}{\partial t}\left(h\left(\frac{1}{2}|\mathbf{u}|^2 + e_i + e_T\right)\right) + \operatorname{div}\left(h\mathbf{u}\left(\frac{1}{2}|\mathbf{u}|^2 + e_i + e_T\right) + \left(\frac{gh^2}{2}\mathbf{I} + h\mathbf{P}\right)\mathbf{u}\right) = 0, \tag{2}$$

where

$$e_T = \frac{1}{2}\operatorname{tr}\mathbf{P}, \quad e_i = \frac{1}{2}gh,$$

and an additional conservation law:

$$\frac{\partial h\Psi}{\partial t} + \operatorname{div}(h\mathbf{u}\Psi) = 0, \ \Psi = \frac{Det(\mathbf{P})}{h^2}. \tag{3}$$

The variable Ψ will be referred to as 'entropy' (mathematical) because this quantity is transported along the mean flow in the same way as the true entropy for the Euler equations of compressible fluids. Also, we will see that this quantity will increase across the shocks in analogy with the conventional entropy (see [38–40] for $1D$ study of roll waves and hydraulic jumps).

The system is hyperbolic but not in conservative form. The hyperbolicity was established, for example, in [8], for the equations of compressible turbulent flows, generalizing system (1). However, the non-conservativity property was just a

[1] The evolution of $\mathbf{P}$ (the last equation of (1)) is not governed by any specific objective derivative, i.e. the equation is not invariant under the change of variables $t' = t$, $\mathbf{x}' = \mathbf{O}(t)\mathbf{x}$, $\mathbf{u}' = \mathbf{O}(t)\mathbf{u} + \dot{\mathbf{O}}\mathbf{x}$, $\mathbf{P}' = \mathbf{O}\mathbf{P}\mathbf{O}^T$. Here $\mathbf{O}(t)$ is a time-dependent orthogonal transformation: $\mathbf{O}\mathbf{O}^T = \mathbf{I}$, 'T' means transposition, and 'dot' denotes the time derivative. This is due to the fact that the tensor equation for the Reynolds stress tensor is not a geometric equation, but a physical one, representing a sort of 'micro' Newton's law derived from the Euler equations by depth averaging. Thus, this equation should be only Galilean invariant, which is obviously the case.

'feeling' which was not rigorously proved in the literature. In Appendix A we prove that (1) admits only five conservation laws written above: conservation of mass, momentum, energy and 'entropy'. Since the number of scalar unknowns is six (h, $\mathbf{u}$ and three independent components of $\mathbf{P}$), the system is not in conservative form. The definition and computation of discontinuous solutions for non-conservative hyperbolic equations is a challenging problem (see examples of non-conservative systems in compressible turbulence [8,2], multi-layer shallow water flows [35,4,33,6,1,31], multi-phase fluid flows [3,26,42–44,20,15], solid-fluid systems [18,34]).

Essentially, four approaches are commonly used for numerical solving of non-conservative systems of equations. The most classical one is based on the definition of non-conservative products proposed by Volpert (Volpert's path) [16]. The second one is the formulation of an augmented system of 'Rankine–Hugoniot relations' through the study of travelling wave solutions of an extended system of equations approximating a given system (formulation of kinetic relations) [52,27]. The third one is based on the relaxation technique: the governing system of equations is approximated by a new hyperbolic system where all eigenfields are linearly degenerate in the sense of Lax [10,15]. Finally, the additional relations can be formulated from the compatibility between theoretical and experimental results [17,44]. Excepting the first approach (more formal and hence less precise), all the approaches mentioned above are not universal: they are usually specific to the model under study.

In [19], a new splitting approach for the modelling of $3D$ isotropic hyperelastic materials was proposed. The model admits three types of sonic waves (one longitudinal and two transverse) and contact characteristics. The system was split into several subsystems each of which contained only one type of sonic waves (only longitudinal or transverse). Each subsystem was hyperbolic and admitted a weak formulation. Such an approach was further extended to the modelling of multi-solid materials [34]. The splitting procedure allowed us not only to define the non-conservative products, but also to increase the precision and robustness of the numerical method. Such a philosophy will also be developed here.

In section 2, the hyperbolicity of system (1) is established. The Rankine–Hugoniot relations compatible to the positive definiteness of the Reynolds stress tensor are proposed in section 3. Dissipation terms are introduced in section 4. The splitting procedure and its numerical realisation are presented in sections 5, 6, 7. The numerical results are presented in section 8. Technical details can be found in Appendices A and B.

2. Hyperbolicity study

The hyperbolicity study is analogous to that given in [8] for the compressible turbulent flows. For completeness, we briefly describe the main results. Denoting the components of $\mathbf{P}$ by P_{ij}, $i, j = 1, 2$, one can rewrite system (1) in Cartesian coordinates in the form:

$$
\begin{aligned}
&h_t + uh_x + vh_y + hu_x + hv_y = 0, \\
&u_t + uu_x + vu_y + gh_x + \frac{1}{h}(hP_{11})_x + \frac{1}{h}(hP_{12})_y = 0, \\
&v_t + uv_x + vv_y + gh_y + \frac{1}{h}(hP_{12})_x + \frac{1}{h}(hP_{22})_y = 0, \\
&P_{11t} + uP_{11x} + vP_{11y} + 2P_{11}u_x + 2P_{12}u_y = 0, \\
&P_{12t} + uP_{12x} + vP_{12y} + P_{12}(u_x + v_y) + P_{11}v_x + P_{22}u_y = 0, \\
&P_{22t} + uP_{22x} + vP_{22y} + 2P_{12}v_x + 2P_{22}v_y = 0.
\end{aligned}
\tag{4}
$$

Or, in matrix form:

$$
\frac{\partial \mathbf{W}}{\partial t} + \mathbf{A}\frac{\partial \mathbf{W}}{\partial x} + \mathbf{B}\frac{\partial \mathbf{W}}{\partial y} = \mathbf{0},
$$

where

$$
\mathbf{W} = \begin{pmatrix} h \\ u \\ v \\ P_{11} \\ P_{12} \\ P_{22} \end{pmatrix}, \quad
\mathbf{A} = \begin{pmatrix}
u & h & 0 & 0 & 0 & 0 \\
\frac{gh + P_{11}}{h} & u & 0 & 1 & 0 & 0 \\
\frac{P_{12}}{h} & 0 & u & 0 & 1 & 0 \\
0 & 2P_{11} & 0 & u & 0 & 0 \\
0 & P_{12} & P_{11} & 0 & u & 0 \\
0 & 0 & 2P_{12} & 0 & 0 & u
\end{pmatrix},
\tag{5}
$$

$$\mathbf{B}=\begin{pmatrix} v & 0 & h & 0 & 0 & 0 \\ \frac{P_{12}}{h} & v & 0 & 0 & 1 & 0 \\ \frac{gh+P_{22}}{h} & 0 & v & 0 & 0 & 1 \\ 0 & 2P_{12} & 0 & v & 0 & 0 \\ 0 & P_{22} & P_{12} & 0 & v & 0 \\ 0 & 0 & 2P_{22} & 0 & 0 & v \end{pmatrix}. \tag{6}$$

The characteristic surfaces $S(t,x,y)=0$ for (4) satisfy the relation [37]:

$$\det\left(\mathbf{I}\frac{\partial S}{\partial t}+\mathbf{A}\frac{\partial S}{\partial x}+\mathbf{B}\frac{\partial S}{\partial y}\right)=0.$$

It implies:

$$\chi=0, \tag{7}$$

$$\chi=\pm\sqrt{(\nabla S)^T\mathbf{P}\nabla S}, \tag{8}$$

$$\chi=\pm\sqrt{gh|\nabla S|^2+3\,(\nabla S)^T\mathbf{P}\nabla S}, \tag{9}$$

where

$$\chi=\frac{\partial S}{\partial t}+\mathbf{u}\cdot\nabla S,\ \nabla S=\left(\frac{\partial S}{\partial x},\frac{\partial S}{\partial y}\right)^T.$$

The characteristic value (7) is double. The characteristic values (8) and (9) are simple and real since $\mathbf{P}$ is positive definite. One can prove that for the double root one has two left linearly independent eigenvectors of the corresponding characteristic matrix. Hence, the equations are hyperbolic.

To understand the structure of the eigenfields, consider the governing equations in x-direction. The eigenvalues of the matrix $\mathbf{A}$ are:

$$\lambda_{1,2}=u,\quad \lambda_{3,4}=u\pm b,\ b=\sqrt{P_{11}},\quad \lambda_{5,6}=u\pm a,\ a=\sqrt{gh+3P_{11}}. \tag{10}$$

For the multiple eigenvalue $\lambda_{1,2}=u$ we have two linearly independent right eigenvectors $\mathbf{r}_i$, $i=1,2$, of $\mathbf{A}$:

$$\begin{aligned} \mathbf{r}_1&=(0,0,0,0,0,1)^T, & \nabla_{\mathbf{W}}\lambda_1\cdot\mathbf{r}_1=0,\\ \mathbf{r}_2&=(-h,0,0,gh+P_{11},P_{12},0)^T, & \nabla_{\mathbf{W}}\lambda_2\cdot\mathbf{r}_2=0. \end{aligned} \tag{11}$$

Here and further, $\nabla_{\mathbf{W}}$ means the gradient operator with respect to $\mathbf{W}$. For the eigenvalue $\lambda_3=u+b$ one has:

$$\mathbf{r}_3=(0,0,b,0,b^2,2P_{12})^T,\quad \nabla_{\mathbf{W}}\lambda_3\cdot\mathbf{r}_3=0. \tag{12}$$

For the eigenvalue $\lambda_4=u-b$ one has:

$$\mathbf{r}_4=(0,0,-b,0,b^2,2P_{12})^T,\quad \nabla_{\mathbf{W}}\lambda_4\cdot\mathbf{r}_4=0. \tag{13}$$

For the eigenvalue $\lambda_5=u+a$ one has:

$$\begin{aligned} \mathbf{r}_5&=\left\{h,\ a,\ \frac{2aP_{12}}{a^2-b^2},\ 2b^2,\ \frac{a^2+b^2}{a^2-b^2}P_{12},\ \frac{4P_{12}^2}{a^2-b^2}\right\}^T,\\ \nabla_{\mathbf{W}}\lambda_5\cdot\mathbf{r}_5&=\frac{3}{2a}\left(a^2+b^2\right)>0. \end{aligned} \tag{14}$$

For the eigenvalue $\lambda_6=u-a$ one has:

$$\begin{aligned} \mathbf{r}_6&=\left\{h,\ -a,\ -\frac{2aP_{12}}{a^2-b^2},\ 2b^2,\ \frac{a^2+b^2}{a^2-b^2}P_{12},\ \frac{4P_{12}^2}{a^2-b^2}\right\}^T,\\ \nabla_{\mathbf{W}}\lambda_6\cdot\mathbf{r}_6&=-\frac{3}{2a}\left(a^2+b^2\right)<0. \end{aligned} \tag{15}$$

Thus, the fields corresponding to the eigenvalues $\lambda_{1,2,3,4}$ are linear degenerate in the sense of Lax, while the fields $\lambda_{5,6}=u\pm a$ are genuinely non-linear. The family $\lambda_{3,4}=u\pm b$ (further on referred to as *b-waves*) is reminiscent of the shear waves in hyperelasticity, while the family $\lambda_{5,6}=u\pm a$ (further on referred to as *a-waves*) is reminiscent of the longitudinal waves. The analogy with shear waves in hyperelasticity and *b*-waves was also noticed in [51] in the case of incompressible Reynolds-averaged Euler equations. An interesting analogy between the linearised equations of incompressible turbulence and Maxwell's equations was also underlined there.

3. Rankine–Hugoniot relations

Since the number of scalar conservation laws is only five (mass, momentum, energy and 'entropy'), while the number of unknowns is six (h, $\mathbf{u}$ and three independent components of $\mathbf{P}$), the system is not in conservative form (see Appendix A for a proof).

For discontinuous solutions, the Rankine–Hugoniot relations coming from the mass, momentum and energy equations are:

$$[h(\mathbf{u}\cdot\mathbf{n}-D_n)]=0,$$
$$\left[h\mathbf{u}(\mathbf{u}\cdot\mathbf{n}-D_n)+\frac{gh^2}{2}\mathbf{n}+h\mathbf{P}\mathbf{n}\right]=0,$$
$$\left[h(\mathbf{u}\cdot\mathbf{n}-D_n)\left(\frac{1}{2}|\mathbf{u}|^2+e_i+e_T\right)+\mathbf{n}^T\left(\frac{gh^2}{2}\mathbf{I}+h\mathbf{P}\right)\mathbf{u}\right]=0.$$

Here for any function f we denote $[f]=f^+-f^-$, where f^+, f^- are the right and the left limit values of f at the discontinuity surface, D_n is the normal velocity of the surface, and $\mathbf{n}$ is the normal unit vector to the surface. We denote also by $\mathbf{s}$ the tangent unit vector to the surface such that $(\mathbf{n},\mathbf{s})$ form a Cartesian basis. Using

$$\mathbf{u}=(\mathbf{u}\cdot\mathbf{n})\mathbf{n}+(\mathbf{u}\cdot\mathbf{s})\mathbf{s},$$

one obtains from the momentum equation the following two scalar relations:

$$\left[h(\mathbf{u}\cdot\mathbf{n}-D_n)^2+\frac{gh^2}{2}+h\mathbf{n}^TP\mathbf{n}\right]=0,$$
$$[h(\mathbf{u}\cdot\mathbf{n}-D_n)(\mathbf{u}\cdot\mathbf{s})+h\mathbf{s}^TP\mathbf{n}]=0.$$

As usually, we distinguish two types of discontinuities: *contact discontinuities* (*interfaces*) where $\mathbf{u}\cdot\mathbf{n}-D_n=0$, and *shock waves* where $\mathbf{u}\cdot\mathbf{n}-D_n\neq 0$.

3.1. Contact discontinuities

We consider first the interfaces $\mathbf{u}\cdot\mathbf{n}-D_n=0$. The momentum equation is equivalent to:

$$\left[\frac{gh^2}{2}+h\mathbf{n}^T\mathbf{P}\mathbf{n}\right]=0,$$
$$[h\mathbf{s}^T\mathbf{P}\mathbf{n}]=0.$$

The energy equation implies:

$$[h(\mathbf{u}\cdot\mathbf{s})\mathbf{s}^T\mathbf{P}\mathbf{n}]=0.$$

We need to distinguish two types of contact discontinuities. The first type is determined by the condition that *at each side of the contact discontinuity the tangential component of the stress vector* $h\mathbf{s}^T\mathbf{P}\mathbf{n}$ *vanishes*. Then, *a priori,* the jump of the tangential velocity can be arbitrary:

$$[\mathbf{u}\cdot\mathbf{s}]\neq 0. \tag{16}$$

So, the sliding is admitted as in the case of contact discontinuities for the Euler equations of compressible fluids.

For the second type of contact discontinuity where the tangential component of the stress vector $h\mathbf{s}^T\mathbf{P}\mathbf{n}$ is continuous, but not necessarily vanishing, the sliding is forbidden:

$$[\mathbf{u}\cdot\mathbf{s}]=0. \tag{17}$$

So, the full velocity vector should be continuous. This kind of interfaces is not admitted by the Euler equations of compressible fluids.

3.2. Shocks

Consider now the discontinuity interfaces where $\mathbf{u}\cdot\mathbf{n} - D_n \neq 0$. They are called *shocks*. The Rankine–Hugoniot relations coming from the mass, momentum (two scalar relations) and energy equations are:

$$
\begin{aligned}
&[h(\mathbf{u}\cdot\mathbf{n} - D_n)] = 0,\\
&\left[h(\mathbf{u}\cdot\mathbf{n} - D_n)^2 + \frac{gh^2}{2} + h\mathbf{n}^T P\mathbf{n}\right] = 0, \quad \left[h(\mathbf{u}\cdot\mathbf{n} - D_n)(\mathbf{u}\cdot\mathbf{s}) + h\mathbf{s}^T P\mathbf{n}\right] = 0,\\
&\left[h(\mathbf{u}\cdot\mathbf{n} - D_n)\left(\frac{1}{2}|\mathbf{u}|^2 + e_i + e_T\right) + (\mathbf{u}\cdot\mathbf{n})\left(\frac{gh^2}{2} + h\mathbf{n}^T\mathbf{P}\mathbf{n}\right) + (\mathbf{u}\cdot\mathbf{s})h\mathbf{s}^T\mathbf{P}\mathbf{n}\right] = 0.
\end{aligned}
$$

Contrary to the Euler equations of compressible fluids, the sliding along the shocks surfaces is not forbidden. This system of Rankine–Hugoniot relations is obviously not sufficient to describe the full structure of strong discontinuities. As it is proved in Appendix A all linearly independent conservation laws admitted by the system (1) of the form:

$$\frac{\partial f}{\partial t} + \frac{\partial g_1}{\partial x} + \frac{\partial g_2}{\partial y} = 0,$$

are only those of mass, momentum, energy and $h\Psi$. Here f, g_1, g_2 are functions depending on h, $\mathbf{u}$ and $\mathbf{P}$. Thus, there is no hope to define a 'classical' weak solution to (1). Moreover, the shock relation coming from the equation for Ψ implies the continuity of Ψ across the shocks. However, this condition is not physically acceptable. Indeed, for $1D$ flows the system of Rankine–Hugoniot relations is closed. Moreover, the $1D$ system admits an analogue of Ψ having a clear physical meaning. This quantity is associated with the enstrophy (squared vorticity) and plays the role of 'mathematical entropy': it increases across the shock. For example, for hydraulic jumps the enstrophy increase corresponds to the vorticity creation: a roller appears at the forward slope of the hydraulic jump [38,39]. Note that in [20] a simplified model of multi-phase flows was proposed, and a quantity analogous to Ψ and characterising the micro-energy of interaction between phases was introduced. This quantity was also increasing across the shock.

The non-conservative nature of the multi-dimensional equations of shear shallow water flows represents an enormous difficulty from the mathematical and numerical point of view. Moreover, when the shocks appear, we also should be aware about positive definiteness of $\mathbf{P}$: this property should be guaranteed for the weak solutions. If the solution is smooth, this property is easy to establish. Indeed, the equation for Ψ can be integrated in the Lagrangian coordinates $\mathbf{X}$ related to the mean flow. One can write in the Lagrangian coordinates:

$$\Psi(t, \mathbf{X}) = \Psi(0, \mathbf{X}),$$

or

$$\frac{\lambda_1\lambda_2}{h^2} = \frac{\lambda_{10}\lambda_{20}}{h_0^2},$$

where λ_i, $i = 1, 2$ are eigenvalues of $\mathbf{P}$, and the index 0 corresponds to the initial state. It is then clear that if $\mathbf{P}$ is initially positive, it will be positive for any time, if the solution is smooth.

We will also establish a set of additional Rankine–Hugoniot relations that guarantees the positive definiteness of $\mathbf{P}$ even in the presence of shocks. Dissipative terms compatible with the positive definiteness of $\mathbf{P}$ will also be introduced into the governing equations.

3.2.1. 'Entropy' increase across the shocks: $1D$ case study

This case was already studied in [49,38,39]. Here, we present it for completeness. The governing equations are:

$$\frac{\partial h}{\partial t} + \frac{\partial hu}{\partial x} = 0, \tag{18}$$

$$\frac{\partial hu}{\partial t} + \frac{\partial}{\partial x}\left(hu^2 + \frac{gh^2}{2} + \Phi h^3\right) = 0, \tag{19}$$

$$\frac{\partial}{\partial t}\left(\frac{h}{2}\left(u^2 + gh + \Phi h^2\right)\right) + \frac{\partial}{\partial x}\left(hu\left(\frac{u^2}{2} + gh + \frac{3}{2}\Phi h^2\right)\right) = 0. \tag{20}$$

Here $\Phi = P_{11}/h^2$ is a one-dimensional analogue of Ψ (P_{11} is a 'one-dimensional' determinant of $\mathbf{P}$). It conserves along trajectories:

$$\frac{D\Phi}{Dt} = 0. \tag{21}$$

The governing equations (18)–(20) are reminiscent of the Euler equations of compressible fluids with the specific internal energy given by:

$$e = \frac{gh}{2} + \frac{\Phi h^2}{2}, \tag{22}$$

and the pressure:

$$p = \frac{gh^2}{2} + \Phi h^3. \tag{23}$$

The enstrophy Φ increases across the shock as the conventional entropy for the Euler equations. Thus, P_{11} remains positive across the shock if it was initially positive.

3.2.2. 'Entropy' increase across the shocks: 2D case study

The previous $1D$ study suggests us a hypothesis about the following set of Rankine–Hugoniot relations. Let us suppose that

$$\left[\frac{\mathbf{s}^T P\mathbf{n}}{h}\right] = 0, \tag{24}$$

$$[\mathbf{s}^T P\mathbf{s}] = 0. \tag{25}$$

Then the 'entropy' Ψ of the system is increasing across the shock if and only if $\frac{\mathbf{n}^T P\mathbf{n}}{h^2}$ is increasing across the shock. Indeed, this fact follows from the inequalities:

$$\begin{aligned}\Psi &= \frac{(\mathbf{n}^T P\mathbf{n})(\mathbf{s}^T P\mathbf{s}) - (\mathbf{s}^T P\mathbf{n})^2}{h^2} = \left(\frac{\mathbf{n}^T P\mathbf{n}}{h^2}\right)\left(\mathbf{s}^T P\mathbf{s}\right) - \left(\frac{(h\mathbf{s}^T P\mathbf{n})^2}{h^4}\right) \\ &= \left(\frac{\mathbf{n}^T P\mathbf{n}}{h^2}\right)\left(\mathbf{s}^T P\mathbf{s}\right)_0 - \left(\frac{(h\mathbf{s}^T P\mathbf{n})^2}{h^4}\right)_0 > \left(\frac{\mathbf{n}^T P\mathbf{n}}{h^2}\right)_0\left(\mathbf{s}^T P\mathbf{s}\right)_0 - \left(\frac{(h\mathbf{s}^T P\mathbf{n})^2}{h^4}\right)_0 = \Psi_0.\end{aligned} \tag{26}$$

Here the index '0' denotes the state before the shock. The justification of the jump relations (24), (25) which guarantees the inequality (26) will be done below by using a specific splitting procedure in solving the non-conservative equations.

4. Dissipative terms compatible with the positive definiteness of the Reynolds stress tensor

We add now dissipative terms in the model:

$$\begin{aligned}&h_t + \operatorname{div}(h\mathbf{u}) = 0, \\ &(h\mathbf{u})_t + \operatorname{div}(h\mathbf{u}\otimes\mathbf{u} + \frac{gh^2}{2}\mathbf{I} + h\mathbf{P}) = -C_f|\mathbf{u}|\mathbf{u}, \\ &\frac{D\mathbf{P}}{Dt} + \frac{\partial\mathbf{u}}{\partial\mathbf{x}}\mathbf{P} + \mathbf{P}\left(\frac{\partial\mathbf{u}}{\partial\mathbf{x}}\right)^T = \mathcal{D}, \quad \mathcal{D} = \mathcal{D}^T.\end{aligned} \tag{27}$$

Here C_f is the Chézy coefficient, and $\mathcal{D}$ is the dissipation tensor to be defined. The equations (27) should also satisfy the energy conservation law:

$$\frac{\partial}{\partial t}\left(h\left(\frac{1}{2}|\mathbf{u}|^2 + e_i + e_T\right)\right) + \operatorname{div}\left(h\mathbf{u}\left(\frac{1}{2}|\mathbf{u}|^2 + e_i + e_T\right) + \left(\frac{gh^2}{2}\mathbf{I} + h\mathbf{P}\right)\mathbf{u}\right) = -C_f|\mathbf{u}|^3 - Q, \tag{28}$$

where the dissipative source term Q should be positive. The positivity of Q is the analogue of the second law of thermodynamics. The compatibility of (27) and (28) implies the expression for Q in terms of $\mathcal{D}$:

$$\operatorname{tr}(\mathcal{D}) = -\frac{2}{h}Q. \tag{29}$$

The equations for the Reynolds stress tensor $\mathbf{P}$ can be written in Cartesian coordinates as follows:

$$\begin{aligned}&\frac{DP_{11}}{Dt} + 2P_{11}u_x + 2P_{12}u_y = \mathcal{D}_{11}, \\ &\frac{DP_{12}}{Dt} + P_{12}\left(u_x + v_y\right) + P_{11}v_x + P_{22}u_y = \mathcal{D}_{12}, \\ &\frac{DP_{22}}{Dt} + 2P_{12}v_x + 2P_{22}v_y = \mathcal{D}_{22}.\end{aligned}$$

Here $\mathcal{D}_{ij}$, $i,j=1,2$ are the components of $\mathcal{D}$. These equations imply the evolution equation for Ψ:

$$h^2\frac{D}{Dt}\left(\frac{P_{11}P_{22}-P_{12}^2}{h^2}\right)=\mathcal{D}_{11}P_{22}-2P_{12}\mathcal{D}_{12}+\mathcal{D}_{22}P_{11}.$$

Or, in invariant form:

$$h^2\frac{D}{Dt}\left(\frac{\det\mathbf{P}}{h^2}\right)=\mathrm{tr}\,(\mathbf{P})\,\mathrm{tr}\,(\mathcal{D})-\mathrm{tr}\,(\mathbf{P}\mathcal{D})\,.$$

By analogy with the Stokes hypotheses, we assume that the dissipation tensor $\mathcal{D}$ is an isotropic tensor function of $\mathbf{P}$. Then, for two-dimensional case, $\mathcal{D}$ is linear in $\mathbf{P}$:

$$\mathcal{D}=-\frac{2}{h}|\mathbf{u}|^3\left(\alpha\mathbf{P}+\frac{\delta}{2}\mathbf{I}\right),$$

where α and δ are functions of invariants of $\mathbf{P}$. The multiplier $-2|\mathbf{u}|^3/h$ is for convenience only. So, α has the dimension s^2m^{-2}, while δ is dimensionless. Consider the simplest case where $\delta=0$. This choice allows us the reduction to the Saint-Venant equations in the limit $\mathbf{P}=\mathbf{0}$. One has finally:

$$\mathcal{D}=-\frac{2\alpha}{h}|\mathbf{u}|^3\mathbf{P}. \tag{30}$$

In particular, this implies the equation for Ψ in the form:

$$h^2\frac{D}{Dt}\left(\frac{\det(\mathbf{P})}{h^2}\right)=-\frac{4\alpha}{h}|\mathbf{u}|^3\det(\mathbf{P})\,. \tag{31}$$

Equations (29) and (30) imply the following relation between Q and α:

$$Q=\alpha\,\mathrm{tr}\,(\mathbf{P})\,|\mathbf{u}|^3. \tag{32}$$

We will finally choose Q as in [39]:

$$\alpha\,\mathrm{tr}\,(\mathbf{P})=max\left(0,C_r\frac{\frac{\mathrm{tr}(\mathbf{P})}{h^2}-\varphi}{\frac{\mathrm{tr}(\mathbf{P})}{h^2}}\right). \tag{33}$$

Here φ and C_r are the model constants: φ is associated with the enstrophy of small vortexes in the vicinity of the bottom, and C_r is the dissipation coefficient associated with the roller formation [38–40]. We will give further the values of these constants evaluated from experimental data. The formula (33) allows us to recover the $1D$ case studied in [39]. As it follows from (31) and (33), 'entropy' Ψ is decreasing on continuous solutions, but always stays positive. This means that the dissipation law also guarantees the positive definiteness of $\mathbf{P}$.

Another choice for the dissipation tensor could also be as follows:

$$\alpha\,\mathrm{tr}\,(\mathbf{P})=C_r. \tag{34}$$

Then

$$Q=C_r|\mathbf{u}|^3,$$

and

$$\mathcal{D}=-\frac{2}{h}C_r|\mathbf{u}|^3\frac{\mathbf{P}}{\mathrm{tr}\,(\mathbf{P})}.$$

Formally, such a choice also guarantees the positive definiteness of $\mathbf{P}$ and thus is reasonable from the physical point of view. However, the wave profiles obtained with such a law do not correspond to the experimental ones. Indeed, Brock [11–13] measured the stationary roll wave profiles in different conditions (different slopes and wall roughness). He noticed that the roll wave profiles contain always the following three essential parts: first, a sudden increase of the depth since all waves break i.e. acquire steeply sloping wave front, second, a continuous zone where the depth increases progressively, and third, a slowly decreasing zone until a new hydraulic jump (see such a profile in Fig. 6). This is the reason to prefer the option (33) because it allows us to reproduce experimental profiles.

5. Splitting method in Cartesian coordinates

For convenience, we write here once again the governing equations (1) in Cartesian coordinates:

$$
\begin{aligned}
&h_t + uh_x + vh_y + hu_x + hv_y = 0,\\
&u_t + uu_x + vu_y + gh_x + \frac{1}{h}(hP_{11})_x + \frac{1}{h}(hP_{12})_y = 0,\\
&v_t + uv_x + vv_y + gh_y + \frac{1}{h}(hP_{12})_x + \frac{1}{h}(hP_{22})_y = 0,\\
&P_{11t} + uP_{11x} + vP_{11y} + 2P_{11}u_x + 2P_{12}u_y = 0,\\
&P_{12t} + uP_{12x} + vP_{12y} + P_{12}\left(u_x + v_y\right) + P_{11}v_x + P_{22}u_y = 0,\\
&P_{22t} + uP_{22x} + vP_{22y} + 2P_{12}v_x + 2P_{22}v_y = 0.
\end{aligned}
$$

As mentioned earlier, the system is hyperbolic but not in conservative form. We will define now an almost conservative formulation of the governing equations based on a splitting procedure. A conventional geometric splitting is first applied: the governing equations are solved first in x and then in y direction. We will do two steps more for each uni-directional subsystem referring to this as a 'physical' splitting. Roughly speaking, each uni-directional subsystem describing two types of waves (surface and shear waves), is split into two subsystems which are hyperbolic and contain only one type of waves (a or b waves). Each physical subsystem admits its own energy conservation law and its own 'entropy'. In physical terms, one can say that one performs a 'thermodynamically compatible' splitting. Analogous approach was proposed in [19].

Consider first the subsystem in x-direction:

$$
\begin{aligned}
&h_t + uh_x + hu_x = 0,\\
&u_t + uu_x + gh_x + \frac{1}{h}(hP_{11})_x = 0,\\
&v_t + uv_x + \frac{1}{h}(hP_{12})_x = 0,\\
&P_{11t} + uP_{11x} + 2P_{11}u_x = 0,\\
&P_{12t} + uP_{12x} + P_{12}u_x + P_{11}v_x = 0,\\
&P_{22t} + uP_{22x} + 2P_{12}v_x = 0.
\end{aligned}
\tag{35}
$$

As mentioned earlier, the system is hyperbolic and admits three types of waves: a contact discontinuity propagating with the velocity u, surface gravity waves propagating with the velocity $u \pm a$, and shear waves propagating with a smaller velocity $u \pm b$. The eigenfields corresponding to the contact discontinuity and *b-waves* are linearly degenerate in the sense of Lax, while the eigenfield corresponding to *a-waves* is genuinely non-linear in the sense of Lax. The idea is to split (35) into two subsystems treating separately *a-waves* and *b-waves*. Subsystem for *a-waves* is:

$$
\begin{aligned}
&h_t + uh_x + hu_x = 0,\\
&u_t + uu_x + gh_x + \frac{1}{h}(hP_{11})_x = 0,\\
&v_t + uv_x = 0,\\
&P_{11t} + uP_{11x} + 2P_{11}u_x = 0,\\
&P_{12t} + uP_{12x} + P_{12}u_x = 0,\\
&P_{22t} + uP_{22x} = 0.
\end{aligned}
\tag{36}
$$

The equations (36) admit the following conservative form:

$$
\begin{aligned}
&h_t + (uh)_x = 0,\\
&(hu)_t + \left(hu^2 + g\frac{h^2}{2} + hP_{11}\right)_x = 0,\\
&(hv)_t + (huv)_x = 0,\\
&\left(h\left(\frac{u^2+v^2}{2} + \frac{gh}{2} + \frac{P_{11}+P_{22}}{2}\right)\right)_t + \left(hu\left(\frac{u^2+v^2}{2} + \frac{gh}{2} + \frac{P_{11}+P_{22}}{2}\right) + \frac{gh^2}{2}u + hP_{11}u\right)_x = 0,\\
&P_{12t} + (uP_{12})_x = 0,\\
&(hP_{22})_t + (huP_{22})_x = 0.
\end{aligned}
\tag{37}
$$

They also admit the 'entropy' equation:

$$\frac{D}{Dt}\left(\frac{P_{11}P_{22}-P_{12}^2}{h^2}\right)=0,\ \frac{D}{Dt}=\frac{\partial}{\partial t}+u\frac{\partial}{\partial x},$$

and the 'enstrophy' equation:

$$\frac{D}{Dt}\left(\frac{P_{11}}{h^2}\right)=0.$$

At this step, one solves six conservation laws (37). The 'entropy' will increase across the shock. Indeed, the ratio P_{12}/h and the component P_{22} are conserved across the shock, so we need only the increase of P_{11}/h^2 what is the case for $1D$ flows [38,39].

The subsystem for *b-waves* is:

$$\begin{aligned}
&h_t=0,\\
&(hu)_t=0,\\
&(hv)_t+(hP_{12})_x=0,\\
&P_{11t}=0,\\
&P_{12t}+P_{11}v_x=0,\\
&P_{22t}+2P_{12}v_x=0.
\end{aligned}\tag{38}$$

An 'almost' conservative form (38) for *b-waves* is:

$$\begin{aligned}
&h_t=0,\\
&(hu)_t=0,\\
&(hv)_t+(hP_{12})_x=0,\\
&P_{11t}=0,\\
&P_{12t}+P_{11}v_x=0,\\
&\left(h\left(\frac{v^2}{2}+\frac{P_{22}}{2}\right)\right)_t+(hP_{12}v)_x=0.
\end{aligned}\tag{39}$$

The shock relation for P_{12} is well defined because for this subsystem P_{11} is continuous across a shock. The 'entropy' conservation law:

$$\frac{\partial}{\partial t}\left(\frac{P_{11}P_{22}-P_{12}^2}{h^2}\right)=0,$$

is a consequence of (39). Since the characteristic field corresponding to *b-waves* is linearly degenerate, the shock velocity will coincide with b. As a consequence, the conservation of energy is equivalent to the conservation of 'entropy'. Thus, the positive definiteness of $\mathbf{P}$ is guaranteed even in the presence of shocks.

The study in y-direction is analogous. Indeed, one has:

$$\begin{aligned}
&h_t+vh_y+hv_y=0,\\
&u_t+vu_y+\frac{1}{h}(hP_{12})_y=0,\\
&v_t+vv_y+gh_y+\frac{1}{h}(hP_{22})_y=0,\\
&P_{11t}+vP_{11y}+2P_{12}u_y=0,\\
&P_{12t}+vP_{12y}+P_{12}v_y+P_{22}u_y=0,\\
&P_{22t}+vP_{22y}+2P_{22}v_y=0.
\end{aligned}\tag{40}$$

The equations for *a-waves* and *b-waves* in y-direction are obtained from the corresponding equations (37) and (39) by the change of variables $u\to v$, $x\to y$, $P_{11}\to P_{22}$, $P_{22}\to P_{11}$.

6. Mathematical properties of split systems

6.1. Subsystem 1 for a-waves

Subsystem (36) can be rewritten in the following form:

$$\frac{\partial \mathbf{W}}{\partial t}+\mathbf{A}(\mathbf{W})\frac{\partial \mathbf{W}}{\partial x}=\mathbf{0}, \tag{41}$$

where the vector of unknowns $\mathbf{W}$ and matrix $\mathbf{A}$ are defined as:

$$\mathbf{W}=(h,u,v,P_{11},P_{12},P_{22})^T,$$

$$\mathbf{A}=\begin{bmatrix} u & h & 0 & 0 & 0 & 0\\ (gh+P_{11})/h & u & 0 & 1 & 0 & 0\\ 0 & 0 & u & 0 & 0 & 0\\ 0 & 2P_{11} & 0 & u & 0 & 0\\ 0 & P_{12} & 0 & 0 & u & 0\\ 0 & 0 & 0 & 0 & 0 & u \end{bmatrix}.$$

The eigenvalues of $\mathbf{A}$ are:

$$\lambda_{1,2,3,4}=u,\ \lambda_{5,6}=u\pm a,\ a=\sqrt{gh+3P_{11}}. \tag{42}$$

For the multiple eigenvalue $\lambda_{1,2,3,4}=u$ we have four linearly independent right eigenvectors of A:

$$\mathbf{r}_1=(h,0,0,-(gh+P_{11}),0,0)^T,\ \nabla_{\mathbf{W}}\lambda_1\cdot\mathbf{r}_1=0,$$
$$\mathbf{r}_2=(0,0,1,0,0,0)^T,\ \nabla_{\mathbf{W}}\lambda_2\cdot\mathbf{r}_2=0,$$
$$\mathbf{r}_3=(0,0,0,0,1,0)^T,\ \nabla_{\mathbf{W}}\lambda_3\cdot\mathbf{r}_3=0,$$
$$\mathbf{r}_4=(0,0,0,0,0,1)^T,\ \nabla_{\mathbf{W}}\lambda_4\cdot\mathbf{r}_4=0.$$

For the eigenvalue $\lambda_5=u+a$ one has:

$$\mathbf{r}_5=(h,a,0,2P_{11},P_{12},0)^T,\quad \nabla_{\mathbf{W}}\lambda_5\cdot\mathbf{r}_5=\frac{3}{2a}\left(a^2+P_{11}\right)>0. \tag{43}$$

For the eigenvalue $\lambda_6=u-a$ one has:

$$\mathbf{r}_6=(h,-a,0,2P_{11},P_{12},0)^T,\quad \nabla_{\mathbf{W}}\lambda_6\cdot\mathbf{r}_6=-\frac{3}{2a}\left(a^2+P_{11}\right)<0. \tag{44}$$

The eigenvectors are linearly independent. Indeed,

$$det\left[\mathbf{r}_1,\mathbf{r}_2,\mathbf{r}_3,\mathbf{r}_4,\mathbf{r}_5,\mathbf{r}_6\right]=-2a^3h\neq 0. \tag{45}$$

Hence, subsystem (41) is hyperbolic.

6.2. Subsystem 2 for b-waves

Subsystem (38) can also be rewritten in the matrix form

$$\frac{\partial \mathbf{W}}{\partial t}+\mathbf{A}(\mathbf{W})\frac{\partial \mathbf{W}}{\partial x}=\mathbf{0},$$

with the matrix $\mathbf{A}$ given by:

$$\mathbf{A}=\begin{bmatrix} 0 & 0 & 0 & 0 & 0 & 0\\ 0 & 0 & 0 & 0 & 0 & 0\\ P_{12}/h & 0 & 0 & 0 & 1 & 0\\ 0 & 0 & 0 & 0 & 0 & 0\\ 0 & 0 & P_{11} & 0 & 0 & 0\\ 0 & 0 & 2P_{12} & 0 & 0 & 0 \end{bmatrix}. \tag{46}$$

It implies:

$$\det(\mathbf{A}-\lambda\mathbf{I})=\lambda^4(P_{11}-\lambda^2)=0. \tag{47}$$

Hence, one has 6 real eigenvalues:

$$\lambda_{1,2,3,4} = 0,\ \lambda_{5,6} = \pm b,\ b = \sqrt{P_{11}}. \tag{48}$$

For the multiple eigenvalue $\lambda_{1,2,3,4} = 0$ one has 4 linearly independent right eigenvectors:

$$\begin{array}{ll} \mathbf{r}_1 = \left(1, 0, 0, 0, -\dfrac{P_{12}}{h}, 0\right)^T, & \nabla_{\mathbf{W}}\lambda_1 \cdot \mathbf{r}_1 = 0, \\ \mathbf{r}_2 = (0, 1, 0, 0, 0, 0)^T, & \nabla_{\mathbf{W}}\lambda_2 \cdot \mathbf{r}_2 = 0, \\ \mathbf{r}_3 = (0, 0, 0, 1, 0, 0)^T, & \nabla_{\mathbf{W}}\lambda_3 \cdot \mathbf{r}_3 = 0, \\ \mathbf{r}_4 = (0, 0, 0, 0, 0, 1)^T, & \nabla_{\mathbf{W}}\lambda_4 \cdot \mathbf{r}_4 = 0. \end{array} \tag{49}$$

For $\lambda_5 = b$ one has:

$$\mathbf{r}_5 = (0, 0, b, 0, b^2, 2P_{12}), \quad \nabla_{\mathbf{W}}\lambda_5 \cdot \mathbf{r}_5 = 0. \tag{50}$$

For $\lambda_6 = -b$ one has:

$$\mathbf{r}_6 = (0, 0, -b, 0, b^2, 2P_{12}), \quad \nabla_{\mathbf{W}}\lambda_6 \cdot \mathbf{r}_6 = 0. \tag{51}$$

The eigenvectors are linearly independent:

$$det\,[\mathbf{r}_1, \mathbf{r}_2, \mathbf{r}_3, \mathbf{r}_4, \mathbf{r}_5, \mathbf{r}_6] = -2P_{11}\sqrt{P_{11}} \neq 0,\ if\ P_{11} \neq 0. \tag{52}$$

Hence, subsystem (38) is hyperbolic.

7. Numerical scheme

The numerical approach for (4) consists in solving first the model in x-direction, and then in y-direction. For each direction, the two subsystems for a- and b-waves are solved successively. A Godunov-type scheme augmented by a correction step (see below) is used for this aim. Finally, the source terms are integrated. The vector of unknowns for all subsystems is:

$$\mathbf{U} = [h, hu, hv, hP_{11}, P_{12}, hP_{22}, hE]^T. \tag{53}$$

Here

$$E = (u^2 + v^2 + gh + P_{11} + P_{22})/2.$$

7.1. First subsystem: a-waves

The first subsystem (called 'subsystem 1') augmented with the energy conservation law for a-waves is:

$$\begin{cases} h_t + (uh)_x = 0, & (a) \\ (hu)_t + \left(hu^2 + p\right)_x = 0, & (b) \\ (hv)_t + (huv)_x = 0, & (c) \\ (hP_{11})_t + (huP_{11})_x + 2hP_{11}u_x = 0, & (d) \\ P_{12t} + (uP_{12})_x = 0, & (e) \\ (hP_{22})_t + (huP_{22})_x = 0. & (f) \\ (hE)_t + (hEu + pu)_x = 0, & (g) \end{cases} \tag{54}$$

with $p = gh^2/2 + hP_{11}$.

The equation (54.d) is not in conservative form, i.e. the product $P_{11}u_x$ is not well defined across discontinuities. Hopefully, this system is overdetermined and the correct value of P_{11} will be obtained using the energy equation (54.g). This system is solved in 3 steps which can be summarized as follows:

- Solve the Riemann problem using any Riemann solver.
- Evolve all conservative variables using the classical Godunov scheme.
- Compute P_{11} from the energy equation.

Each step is detailed hereafter.

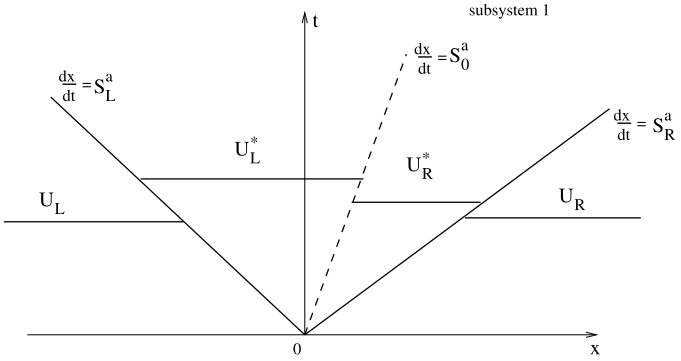

Fig. 1. HLLC approximate Riemann solver for subsystem 1 describing a-waves. The solution in the 'star' region consists of two constant states separated by a middle wave of speed $S_0^a = u^*$. The fastest and slowest waves denoted by S_L^a and S_R^a, respectively, are estimated by using Davis' approximation.

7.1.1. HLLC Riemann solver for subsystem 1

For the first subsystem (54) the wave scheme is shown in Fig. 1. The Rankine–Hugoniot relations read:

$$\begin{aligned}
-[h]\,S^a + [hu] &= 0,\\
-[hu]S^a + \left[hu^2 + p\right] &= 0,\\
-[hv]S^a + [huv] &= 0,\\
-[P_{12}]S^a + [uP_{12}] &= 0,\\
-[hP_{22}]S^a + [huP_{22}] &= 0,\\
-[hE]\,S^a + [hEu + pu] &= 0.
\end{aligned}$$

Here S^a is the discontinuity speed, and $[f]$ means the jump of any variable f. The jump relation for mass equations can be written in the following form:

$$[h(u - S^a)] = 0, \text{ i.e. } h(u - S^a) = m = const.$$

We denote

$$\begin{aligned}
m_L &= h_L(u_L - S_L^a) = h_L^*(u^* - S_L^a)\\
m_R &= h_R(u_R - S_R^a) = h_R^*(u^* - S_R^a).
\end{aligned}$$

Here the speeds of the left and right facing waves are obtained by using Davis' approximation:

$$S_R^a = max(u_L + a_L, u_R + a_R),\ S_L^a = min(u_L - a_L, u_R - a_R),$$

with $a_{L,R}^2 = gh_{L,R} + 3P_{11\,L,R}$. The Rankine–Hugoniot relations imply the continuity of the following parameters in the 'star regions':

$$u_L^* = u_R^* = u^*,\ v_L^* = v_L,\ v_R^* = v_R,\ p_L^* = p_R^* = p^*,$$

with

$$p = \frac{gh^2}{2} + hP_{11}.$$

The momentum conservation law implies:

$$u^* = \frac{p_L - p_R + m_L u_L - m_R u_R}{m_L - m_R},$$

and

$$p^* = \frac{m_L m_R(u_R - u_L) + m_L p_R - p_L m_R}{m_L - m_R}.$$

Finally, the conservative variables in the 'star region' are:

$$\begin{aligned}
h_{L,R}^* &= m_{L,R}/(u^* - S_{L,R}^a),\\
h_{L,R}^* u_{L,R}^* &= \left(h_{L,R}u_{L,R}(u_{L,R} - S_{L,R}^a) + p_{L,R} - p^*\right)/(u^* - S_{L,R}^a),
\end{aligned}$$

$$h^*_{L,R}v^*_{L,R} = h_{L,R}v_{L,R}(u_{L,R} - S^a_{L,R})/(u^* - S^a_{L,R}),$$
$$P^*_{12\,L,R} = P_{12\,L,R}\left(u_{L,R} - S^a_{L,R}\right)/(u^* - S^a_{L,R}),$$
$$h^*_{l,r}E^*_{L,R} = \left(h_{L,R}E_{L,R}(u_{L,R} - S^a_{L,R}) + p_L u_L - p^*u^*\right)/(u^* - S^a_{L,R}).$$

These relations allow us to construct an approximate Riemann solver.

7.1.2. Godunov-type scheme for subsystem 1

Subsystem 1 can be rewritten in the following form:

$$\frac{\partial \mathbf{U}}{\partial t} + \frac{\partial \mathbf{F}}{\partial x} = 0. \tag{55}$$

Here the vector of conservative variables $\mathbf{U}$ and the vector of fluxes $\mathbf{F}$ are:

$$\begin{aligned} \mathbf{U} &= (h, hu, hv, P_{12}, hP_{22}, hE)^T, \\ \mathbf{F}(\mathbf{U}) &= \left(hu, hu^2 + p, huv, uP_{12}, huP_{22}, huE + pu\right)^T. \end{aligned} \tag{56}$$

For simplicity, we use here the same generic notation $\mathbf{U}$ for the vector of conservative variables, even if this vector does not contain the component hP_{11}. Using the flux solution obtained in section 7.1.1 at the edge of each cells ($\mathbf{F}^*$), the conservative variables are evolved as:

$$\mathbf{U}_i^{n+1} = \mathbf{U}_i^n - \frac{\Delta t}{\Delta x}\left(\mathbf{F}^{*,n}_{i+1/2} - \mathbf{F}^{*,n}_{i-1/2}\right). \tag{57}$$

Here Δx is the discretisation step in the x-direction, Δt is the time step verifying the Courant–Friedrichs–Lewy (CFL) condition ($\Delta t \leq \Delta x/S_{max}$). At this step the non-conservative equation for hP_{11} is removed.

7.1.3. Computation of hP_{11}

Since the system is overdetermined, the non-conservative term hP_{11} is obtained by using the total energy equation:

$$hP_{11} = 2hE - gh^2 - hP_{22} - \frac{(hu)^2 + (hv)^2}{h}.$$

7.2. Subsystem 2: b-waves

The subsystem for b-waves (called 'subsystem 2'), augmented with the energy conservation law, reads:

$$\begin{cases} h_t = 0, & (a) \\ (hu)_t = 0, & (b) \\ (hv)_t + (hP_{12})_x = 0, & (c) \\ (hP_{11})_t = 0, & (d) \\ P_{12t} + P_{11}v_x = 0, & (e) \\ (hP_{22})_t + 2hP_{12}v_x = 0, & (f) \\ (hE)_t + (hP_{12}v)_x = 0. & (g) \end{cases} \tag{58}$$

Again, the system (58) is overdetermined. One can note that there are two nonconservative equations (58.e) and (58.f). The product $P_{11}v_x$ in (58.e) is well defined since P_{11} is conserved across the shock. It is not the case for the term $2hP_{12}v_x$ in equation (58.f). Since the jump relation is not well defined, there is no hope to obtain a good value of P_{22}. In the first step, this equation will be removed. Then, the energy conservation law will be again used to compute the value of hP_{22}. The numerical procedure will be similar to a-wave procedure:

- Solve the Riemann problem using any Riemann solver.
- Evolve all conservative variables using the classical Godunov scheme.
- Compute hP_{22} from the energy equation.

These steps and some important remarks on the evolution of the 'entropy' will be detailed hereafter.

7.2.1. HLLC Riemann solver for b-waves

Subsystem 2 for b-waves can be rewritten in the following form:

$$\frac{\partial \mathbf{U}}{\partial t} + \frac{\partial \mathbf{F}}{\partial x} + \mathbf{K}\frac{\partial v}{\partial x} = 0, \tag{59}$$

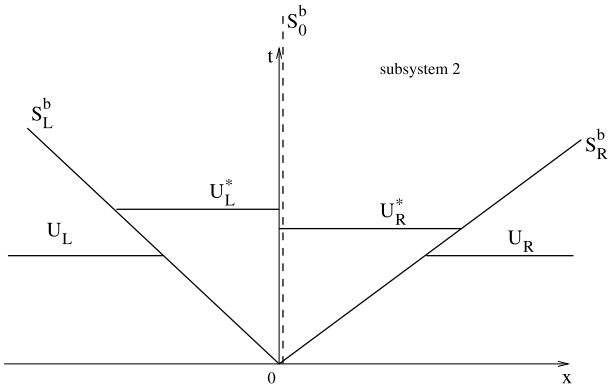

Fig. 2. HLLC approximate Riemann solver for subsystem 2 describing b-waves. Solution in the 'star' region consists of two constant states separated by a middle wave of speed $S_0^b = 0$. The fastest and slowest waves S_R^b and S_L^b, respectively, are estimated by using Davis' approximation.

with

$$\begin{aligned} \mathbf{U} &= (h, hu, hv, hP_{11}, P_{12}, hE)^T, \\ \mathbf{F} &= \mathbf{F}(\mathbf{U}) = (0, 0, hP_{12}, 0, 0, hP_{12}v)^T, \\ \mathbf{K} &= \mathbf{K}(\mathbf{U}) = (0, 0, 0, 0, P_{11}, 0)^T. \end{aligned} \tag{60}$$

Again, for simplicity, the generic notation $\mathbf{U}$ for the 'conservative' vector is used, even if this vector does not contain now the component hP_{22}. The wave scheme is shown in Fig. 2. The set of jump relations for subsystem 2 is:

$$-[h]S^b = 0,\ -[u]S^b = 0,\ -[P_{11}]S^b = 0, \tag{61}$$

$$-[hv]S^b + [hP_{12}] = 0, \tag{62}$$

$$-\left[h\left(\frac{v^2 + P_{22}}{2}\right)\right]S^b + [hvP_{12}] = 0. \tag{63}$$

Across the contact discontinuity ($S^b = 0$) *a priori* one has:

$$[h] \neq 0, \quad [u] \neq 0, \quad [P_{11}] \neq 0, \tag{64}$$

but

$$h_L^* P_{12\,L}^* = h_R^* P_{12\,R}^* = (hP_{12})^*, \quad v^* = v_L^* = v_R^*.$$

Across the shocks ($S^b \neq 0$) one has from (61):

$$h_L = h_L^*, \quad h_R = h_R^*, \quad u_R = u_R^*, \quad P_{11\,R} = P_{11\,R}^*. \tag{65}$$

Equation (62) gives:

$$(hP_{12})^* = h_R h_L \frac{S_R^b P_{12L} - S_L^b P_{12R} - S_L^b S_R^b (v_L - v_R)}{h_R S_R^b - h_L S_L^b}, \tag{66}$$

and

$$v^* = \frac{h_L(P_{12\,L} - S_L^b v_L) - h_R(P_{12\,R} - S_R^b v_R)}{h_R S_R^b - h_L S_L^b}.$$

The extreme wave speeds can be estimated by Davis' approximation:

$$S_L^b = min(-\sqrt{P_{11L}}, -\sqrt{P_{11R}}), \quad S_R^b = max(\sqrt{P_{11L}}, \sqrt{P_{11R}}).$$

Since the eigenfields is linearly degenerate, the wave speed on the right (left) only depend on the right (left) state. Thus, another possibility is:

$$S_L^b = -\sqrt{P_{11\,L}}, \quad S_R^b = \sqrt{P_{11\,R}}. \tag{67}$$

This choice, more precise, is used for all the numerical results presented here. These relations allows us to construct an approximate Riemann solver.

7.2.2. Godunov-type scheme for subsystem 2

The non-conservative equations for P_{12} and P_{22} necessitate a specific numerical treatment. For the equations in conservative form, we use the following Godunov-type scheme:

$$\mathbf{U}_i^{n+1} = \mathbf{U}_i^n + \frac{\Delta t}{\Delta x}(\mathbf{F}_{i+1/2}^{*,n} - \mathbf{F}_{i-1/2}^{*,n}) + \mathbf{K}_i^n (v_{i+1/2}^{*,n} - v_{i-1/2}^{*,n}). \tag{68}$$

7.2.3. Computation of hP_{22}

The non-conservative term hP_{22} is obtained by using the total energy equation:

$$hP_{22} = 2hE - gh^2 - hP_{11} - \frac{(hu)^2 + (hv)^2}{h}. \tag{69}$$

7.2.4. Conservation of the 'entropy'

It is striking that subsystem (58) conserves also the mathematical 'entropy'. Indeed, consider the Rankine–Hugoniot relations:

$$\begin{cases} -[v]S^b + [P_{12}] = 0, \\ -[(v^2 + P_{22})/2]S^b + [P_{12}v] = 0. \end{cases} \tag{70}$$

Here, for any f, $[f] = f - f_0$, where the index '0' means the state before the shock. It implies:

$$\begin{cases} P_{12} = (P_{12})_0 + S^b(v - v_0), \\ P_{22} = (P_{22})_0 + [2P_{12}v]/S^b - [v^2], \end{cases} \tag{71}$$

We will show now that $[\det\mathbf{P}] = 0$. Since h is continuous across the shock, it implies the conservation of the 'entropy'. As P_{11} is continuous, we obtain:

$$\det\mathbf{P} - \det\mathbf{P}_0 = (P_{11})_0 (P_{22} - (P_{22})_0) + ((P_{12})_0 - P_{12})((P_{12})_0 + P_{12}). \tag{72}$$

Replacing (71) into (72) one obtains:

$$\det\mathbf{P} - \det\mathbf{P}_0 = (P_{11})_0 \left(\frac{[2P_{12}v]}{S^b} - [v^2] \right) - S^b[v]\left(2(P_{12})_0 + S^b(v - v_0)\right) =$$

$$= (P_{11})_0 \left(2\frac{\left((P_{12})_0 + S^b(v - v_0)\right)v - (P_{12})_0 v_0}{S^b} - [v^2] \right) - S^b(v - v_0)\left(2(P_{12})_0 + S^b(v - v_0)\right).$$

As $(S^b)^2 = P_{11} = (P_{11})_0$, this can be simplified to:

$$\det\mathbf{P} - \det\mathbf{P}_0 = (P_{11})_0 \left(2(v - v_0)v - (v^2 - v_0^2) - (v - v_0)^2\right) = 0.$$

The mathematical 'entropy' $\Psi = \dfrac{\det\mathbf{P}}{h^2}$ is thus conserved because the corresponding eigenfields are linearly degenerate in the sense of Lax. Finally, the 'entropy' is increasing after solving the first subsystem, and does not change in solving the second subsystem.

7.3. Integration of the source terms

To add the source terms, we integrate the ordinary differential equations:

$$\frac{d\mathbf{U}}{dt} = \mathbf{S}(\mathbf{U}) \tag{73}$$

with the full unknown vector $\mathbf{U} = (h, hu, hv, hP_{11}, P_{12}, hP_{22}, hE)^T$. The initial condition $\mathbf{U}|_{t=0} = \bar{\mathbf{U}}^{n+1}$ are obtained from the previous splitting steps. Here the source term is:

$$\mathbf{S}(\mathbf{U}) = \left(0, -gh\nabla b - C_f\mathbf{u}|\mathbf{u}|, h\mathcal{D}_{11}, \mathcal{D}_{12}, h\mathcal{D}_{22}, -gh\nabla b\cdot\mathbf{u} - C_f|\mathbf{u}|^3 - Q\right)^T, \tag{74}$$

where

$$|\mathbf{u}| = \sqrt{u^2 + v^2},\ \mathcal{D}_{ij} = -\frac{2\alpha}{h}|\mathbf{u}|^3 P_{ij},\ Q = \alpha\mathrm{tr}(\mathbf{P})|\mathbf{u}|^3,$$

$$\alpha\mathrm{tr}(\mathbf{P}) = \max\left(0, C_r\frac{\dfrac{\mathrm{tr}(\mathbf{P})}{h^2} - \varphi}{\dfrac{\mathrm{tr}(\mathbf{P})}{h^2}}\right),\ \nabla b = \left(\frac{\partial b}{\partial x}, \frac{\partial b}{\partial y}\right)^T.$$

We added here the bottom topography $z = b(x, y)$. The equations are written in the reference frame where the gravity is orthogonal to the (x, y)-plane. So, the case of a mild slope bottom is considered. For applications, we will consider only the case of a constant slope bottom:

$$-\nabla b = (\tan\theta,\ 0)\,,\ \theta > 0,$$

where θ is the inclination angle. Even if we have seven equations for six variables, the equations are compatible: the energy equation is a consequence of the equations of mass, momentum and stress.

This system of ordinary differential equation is solved by the first order scheme with the Euler method. A second order Runge–Kutta method is used for the higher order extension.

7.4. Algorithm summary

First, the $2D$ system is split into two $1D$ systems along each spatial direction. Then, each $1D$ system is successively split into two additional $1D$ subsystems. All the systems are hyperbolic. The numerical algorithm can be summarized as follows:

1. Subsystem 1 in x-direction.
   - Solve the Riemann Problem in x-direction for subsystem 1 at each cell boundary without source terms. The approximate HLLC solver was used for this aim.
   - Evolve all flow variables with the Godunov-type method.
   - Correction of the non-conservative variable (hP_{11}) using the energy conservation law.
2. Subsystem 2 in x-direction.
   - Solve the Riemann Problem in x-direction for subsystem 2 at each cell boundary.
   - Evolve for the conservative equations flow variables with the Godunov-type method.
   - The correction of the non-conservative variable (hP_{22}) using energy conservation law.
3. The same procedure is repeated in y-direction by changing $u \to v$, $x \to y$, $P_{11} \to P_{22}$, $P_{22} \to P_{11}$.
4. Integration of the source terms.
5. Start again for the next time step.

8. Numerical results

In this section, we present numerical results obtained with the splitting procedure described above.

8.1. 1D shear test problem

We solve here the governing equations in the case of vanishing source term. The initial discontinuity is located at $x = 0.5$ m. The initial depth h is 0.01 m, the normal velocity u is zero everywhere, the components of the stress tensor are $P_{11} = P_{22} = 10^{-4}\ \mathrm{m}^2/\mathrm{s}^2$, $P_{12} = 0\ \mathrm{m}^2/\mathrm{s}^2$, the tangential velocity v is 0.2 m/s on the left, and -0.2 m/s on the right. The first order Godunov method is used, with CFL number 0.3. The tangential velocity, tangential stress P_{12} and stress P_{22} are shown in Fig. 3 at time instant 10 s for 500, 1000 and 10000 grid cells. The other variables do not evolve in time, they are shown in Fig. 4.

8.2. 1D dam–break problem

We solve here the governing equations in the case of vanishing source term. The initial discontinuity is located at $x = 0.5$ m. The initial normal and tangential velocities are zero everywhere, the components of the stress tensor are: $P_{11} = P_{22} = 10^{-4}\ m^2/s^2$, $P_{12} = 0\ \mathrm{m}^2/\mathrm{s}^2$, the fluid depth is 0.02 m at the left and 0.01 m at the right. The MUSCL extension of Godunov method is used [54]. The results are obtained by using Minmod limiter for subsystem 1, and van Leer limiter for subsystem 2. The solution for 100, 1000 and 10000 grid cells is shown in Fig. 5. The convergence is clearly visible.

8.3. 1D roll waves

We solve here the governing equations with source term. The bottom is inclined either in x-direction, or in y-direction. Using periodic conditions in the direction of wave propagation, and the rigid wall condition in the transverse direction, we observe the formation of roll waves as in [38,25]. The initial conditions are taken in the same form as in the above mentioned references. For example, for the flow in x-direction, one takes:

$$h(x, y, 0) = h_0\left(1 + a\sin\left(\frac{2\pi x}{L_x}\right)\right),\ u(x, y, 0) = \sqrt{\frac{gh_0\tan\theta}{C_f}},\ v(x, y, 0) = 0,$$

$$P_{11}(x, y, 0) = P_{22}(x, y, 0) = \frac{\varphi h^2(x, y, 0)}{2},\ P_{12} = 0.$$

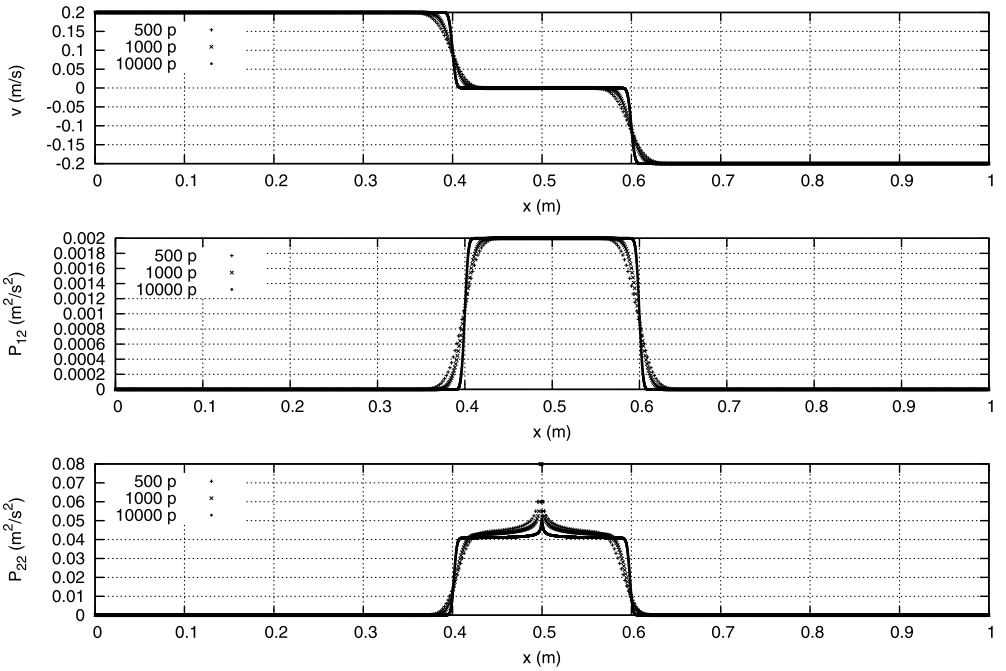

Fig. 3. Shear test problem. The initial discontinuity is located at $x = 0.5$ m. The tangential velocity is 0.2 m/s on the left, and -0.2 m/s on the right. The tangential velocity, shear stress P_{12} and stress P_{22} are shown at time instant 10 s for 500, 1000 and 10000 grid cells. CFL number is 0.3.

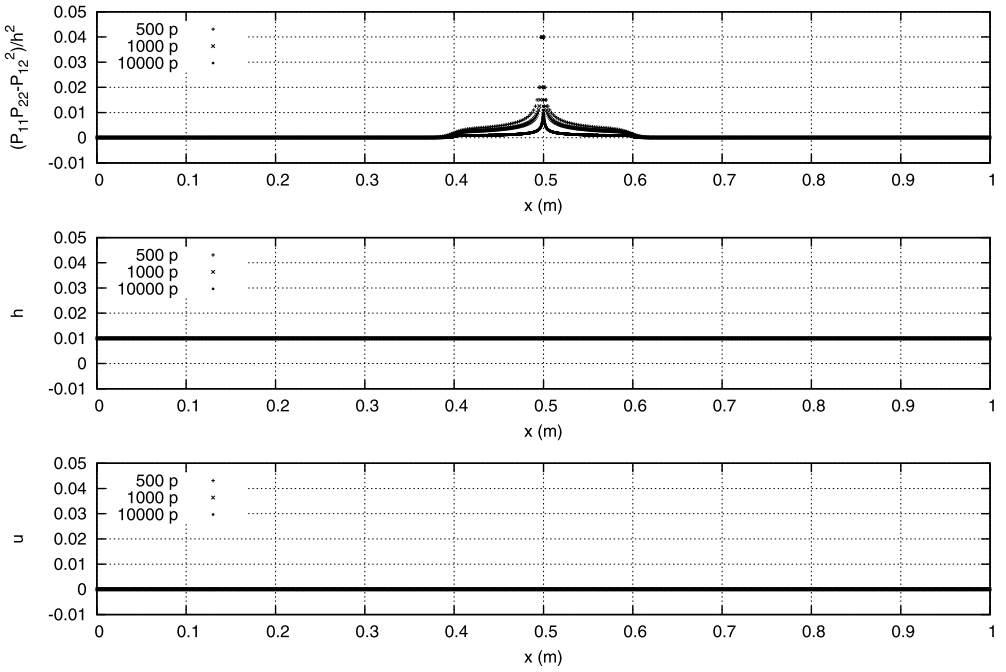

Fig. 4. Shear test problem: initially, the discontinuity of the tangential velocity (0.2 m/s on the left and -0.2 m/s on the right) is at $x = 0.5$ m. The 'entropy', depth and normal velocity are shown at time instant 10 s for 500, 1000 and 10000 grid cells. CFL number is 0.3.

Here $\theta = 0.05011$ [rad] is the inclination angle, $C_f = 0.0036$ is the Chézy coefficient, $h_0 = 7.98 \times 10^{-3}$ m, $a = 0.05$, $\varphi = 22.76\ \mathrm{s}^{-2}$, $g = 9.81\ \mathrm{m\,s}^{-2}$, $C_r = 0.00035$, $L_x = 1.3$ m. For the flow in y-direction the changes in initial conditions are obvious.

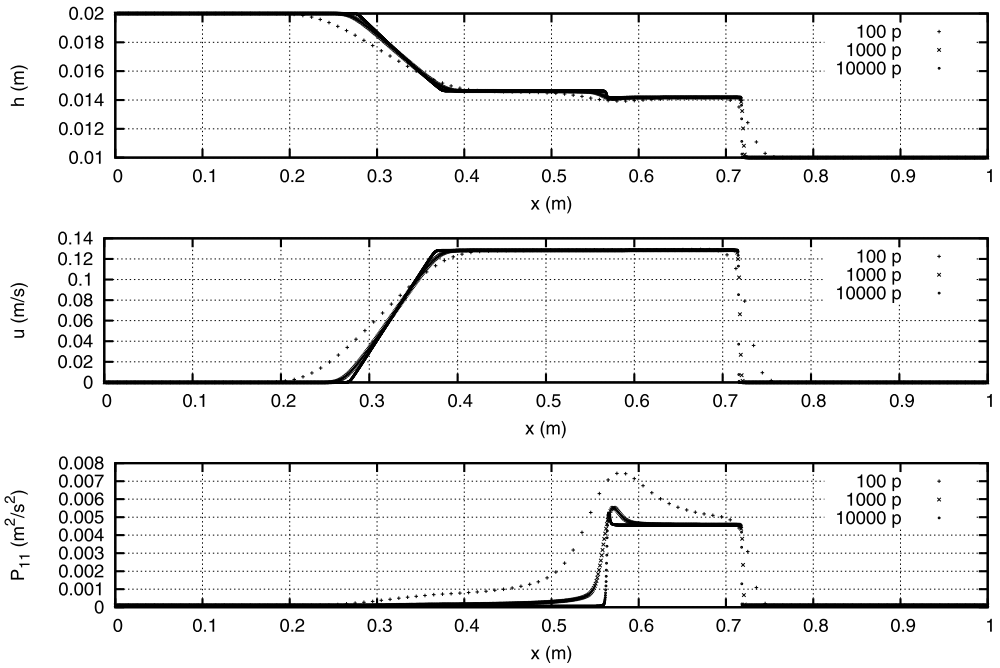

Fig. 5. Convergence test in dam–break problem: the initial discontinuity of the depth (0.02 m at the left and 0.01 m at the right) is located at $x = 0.5$ m. The fluid depth, normal stress component P_{11} and normal velocity u are shown at time instant 0.5 s with 100, 1000 and 10000 grid cells. The MUSCL extension of Godunov method is used. CFL number is 0.8.

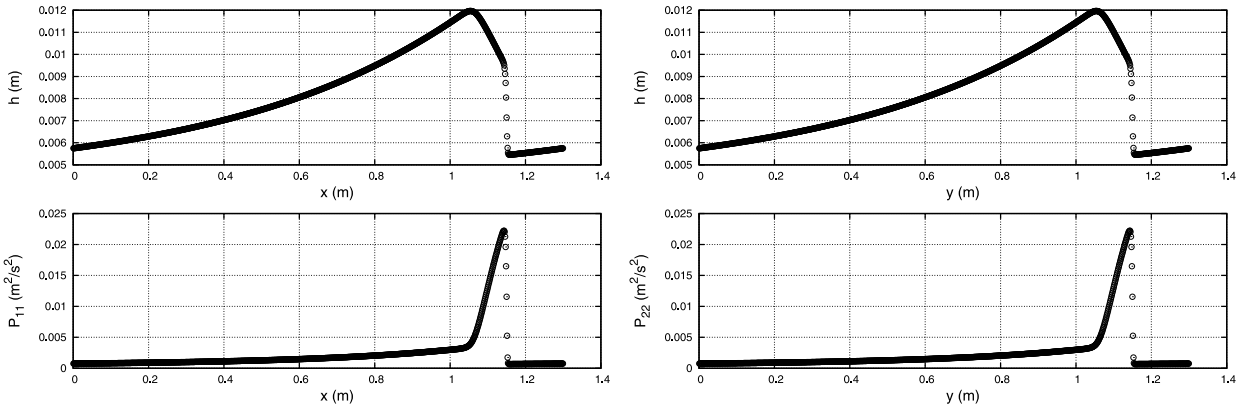

Fig. 6. Formation of roll waves: the depth and normal stress are shown at time instant 25 s for flows both in x- and y-direction (on the left and on the right, respectively). The results are completely symmetric. The MUSCL extension of Godunov method was used with 1000 grid cells for the parameter set mentioned above. CFL number is 0.6.

8.4. Comparison with a 2D analytical solution

Here we present an analytical solutions to (1). This solution is a generalisation of solutions with linear velocity profile in x an y found by Sedov [45] and Ovsyannikov [36] for the Euler equation (for proof, see Appendix B):

$$\begin{cases} h = \dfrac{h_0}{1+\beta^2 t^2}, \\ \mathbf{U} = \dfrac{\beta}{1+\beta^2 t^2}\begin{pmatrix} \beta t x + y \\ -x + \beta t y \end{pmatrix}, \\ \mathbf{P} = \dfrac{1}{(1+\beta^2 t^2)^2}\begin{pmatrix} \lambda + \gamma\beta^2 t^2, & (\lambda-\gamma)\beta t \\ (\lambda-\gamma)\beta t, & \gamma + \lambda\beta^2 t^2 \end{pmatrix}, \end{cases} \tag{75}$$

where $h_0 > 0$, β, $\lambda > 0$, $\gamma > 0$ are constant. The stress tensor $\mathbf{P}$ is not spherical. We take here $h_0 = 1$ m, $\lambda = 0.1$ m^2/s^2, $\gamma = 0.01$ m^2/s^2, $\beta = 10^{-3}$ s^{-1}, $CFL = 0.5$. The L_1-error is calculated at time instant 10 s in the following way:

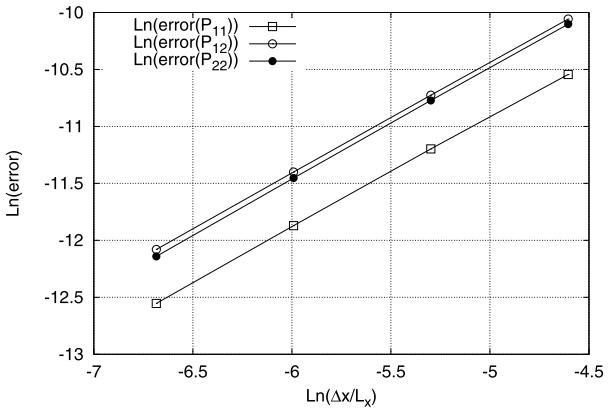

Fig. 7. The convergence lines for the stress tensor components as functions of the grid cell size Δx are shown. The number of grid cells was 100×100, 200×200, 400×400, 800×800. The convergence to the exact solution is clearly visible.

$$error(P_{11}) = \frac{1}{\lambda N_x N_y} \sum_{i,j=1}^{N_x,N_y} |P_{11numerical}(i,j) - P_{11analytical}(i,j)|,$$

$$error(P_{12}) = \frac{1}{(\lambda+\gamma) N_x N_y} \sum_{i,j=1}^{N_x,N_y} |P_{12numerical}(i,j) - P_{12analytical}(i,j)|,$$

$$error(P_{22}) = \frac{1}{\gamma N_x N_y} \sum_{i,j=1}^{N_x,N_y} |P_{22numerical}(i,j) - P_{22analytical}(i,j)|.$$

The computation domain D is a square of length $L_x = L_y = 10$ m, and N_x (N_y) is the number of mesh cells in x (y)-direction. These errors are shown in Fig. 7 as functions of the grid cell size Δx. Different regular Cartesian grids were used (100×100, 200×200, 400×400, 800×800) with first order Godunov method. This test shows the convergence to the exact solution. The slope of the convergence lines are the same for all stress components.

8.5. 2D roll waves

We solve here the $2D$ governing equations with source term. The bottom is inclined in x-direction. In the direction of wave propagation we use periodic conditions for the vector of unknowns ($\mathbf{U}(0,y,t) = \mathbf{U}(L_x,y,t)$), and in the transverse direction we use the rigid wall conditions ($v(x,0,t) = v(0,L_y,t) = 0$, $P_{12}(x,0,t) = P_{12}(x,L_y,t) = 0$, $P_{22}(x,0,t) = P_{22}(x,L_y,t) = 0$, and Neumann conditions for other variables). The initial conditions are taken in the form:

$$h(x,y,0) = h_0\left(1 + a\sin\left(\frac{2\pi m x}{L_x}\right) + a\sin\left(\frac{2\pi k y}{L_y}\right)\right),\ u(x,y,0) = \sqrt{\frac{g h_0 \tan\theta}{C_f}},\ v(x,y,0) = 0, \tag{76}$$

$$P_{11}(x,y,0) = P_{22}(x,y,0) = \frac{\varphi h^2(x,y,0)}{2},\ P_{12} = 0.$$

Here $a = 0.05$ is the perturbation amplitude, $\theta = 0.05011$ [rad] is the inclination angle, $C_f = 0.0036$ is the Chézy coefficient, $h_0 = 7.98 \times 10^{-3}$ m, $\varphi = 22.76\ \mathrm{s}^{-2}$, $g = 9.81\ \mathrm{m\,s}^{-2}$, $C_r = 0.00035$, $L_x = 1.3$ m, $L_y = 0.5$ m, and m and k are numbers to be chosen. The set of physical parameters corresponds to that considered in [25] to describe the formation of $1D$ roll waves from a uniform flow having the same structure as in Brock's experiments [11–13]. A necessary condition for the formation of such waves is that the corresponding Froude number is larger than two: $F_g = \sqrt{\frac{g h_0 \tan(\theta)}{C_f (g h_0 + 3\varphi h_0^2/2)}} > 2$. For the flow parameters taken above, this value is about 3.7.

Fig. 8 shows the convergent numerical solution obtained from a uniform flow perturbed both in x and y direction with $m = 1$ and $k = 1$ (see initial data (76)). The existence of a characteristic transverse wave length of the jump toe perimeter (the line where the gradient of the layer thickness h jumps) is clearly visible. One can count approximately 7 transverse waves.

The transverse structure formation scenario is rather surprising. First, a one-dimensional roll wave is forming, without any transverse structure. This $1D$ structure is formed in approximately 10 s and corresponds to a standard $1D$ experimental profile [11–13] (see Fig. 9). The transverse structure starts to form in approximately 17 s and becomes stationary after

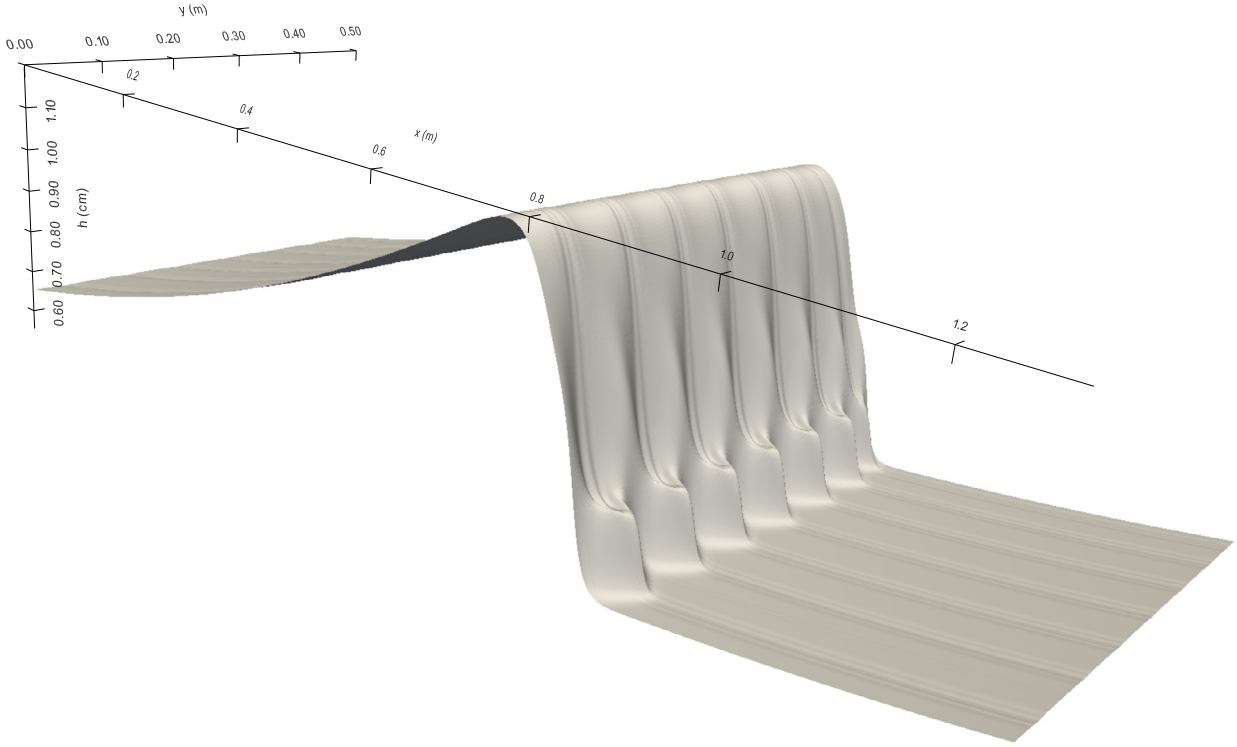

Fig. 8. Formation of transverse structures at the jump toe perimeter consisting of seven waves for the initial data (76) with $m = 1$ and $k = 1$. The convergent solution is obtained for the domain 1.3 m long and 0.5 m wide and shown at time instant 39 s. The Godunov method was used with 600×600 grid cells for the parameter set mentioned above. CFL number is 0.1.

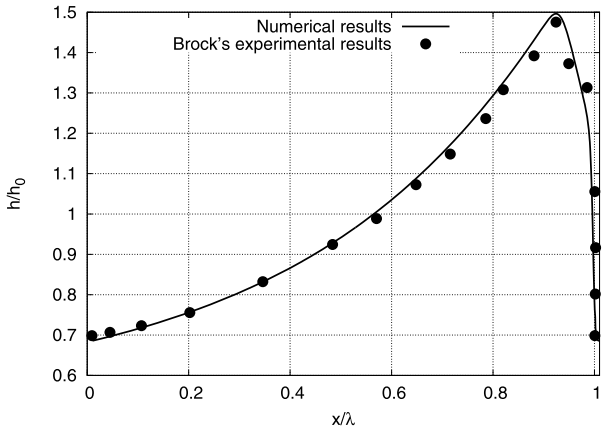

Fig. 9. The one-dimensional wave structure is formed in approximately 10 s (solid line) and corresponds to the classical experilmental profile (dots) measured in [11–13].

approximately 35 s. Thus, the whole scenario is described: from uniform unstable flow to $1D$ roll waves, and finally to the formation of transverse jump toe perimeter profiles (formation of 'fingers'). 'Fingering' of the bore toe perimeter was already observed, in particular, in field experiments [28].

To understand if the number of transverse waves per unit length is independent on the initial perturbations, we considered also the initial data (76) with $m = 1$ and $k = 4$. Thus, the initial transverse perturbation contains four waves, and one could expect that the number of transverse waves formed during the evolution will increase. The result is rather surprising: the number of waves is almost independent on the initial perturbation, only approximately eight waves were formed instead of seven (see Fig. 10).

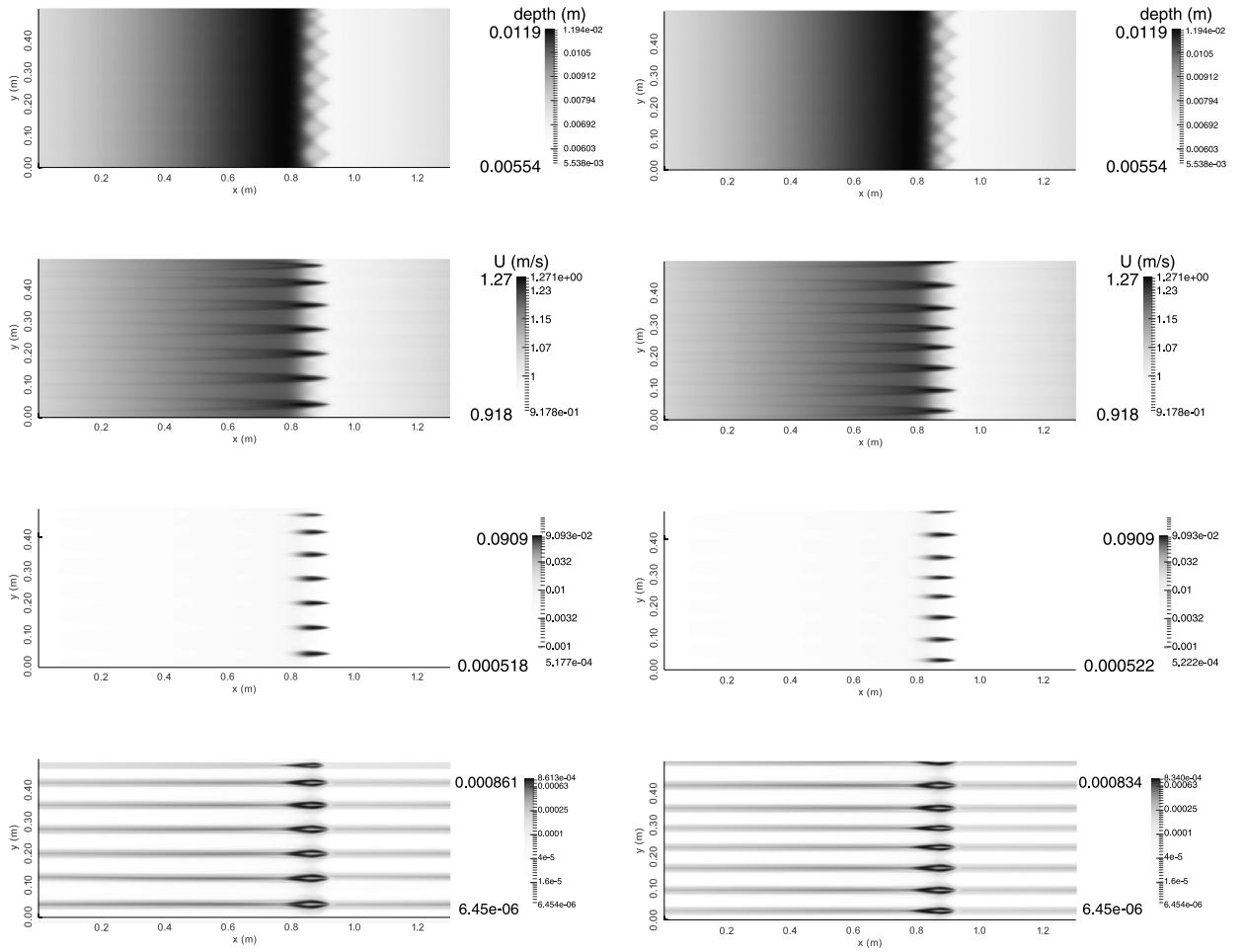

Fig. 10. Top view for the schlieren image of the fluid depth, horizontal velocity, and normal stress components P_{11} and P_{22} for the initial perturbation (76) with $k = 1$, $m = 1$ (on the left) and $k = 1$, $m = 4$ (on the right) at time instant 39 s. The computational domain is 1.3 m long and 0.5 m wide. The Godunov method was used, with 600×600 grid cells for the parameter set mentioned above. CFL number here is 0.1. Seven transverse waves are observed on the left, and almost eight waves on the right.

An additional test was also performed to show that the number of transverse waves per unit length is invariant with respect to the domain width. For this, we multiplied the length L_y by two ($L_y = 1$ m), and took $m = 1$, $k = 1$. As a consequence, the number of transverse waves was also multiplied by two (see Figs. 11 and 12).

The form of the dissipation term defined by the coefficient α given by (33) is very important. Indeed, this form was chosen to obtain the same dissipation source term Q as in $1D$ case studied in [38,39]. A simplified formula for α (34) will give us only $1D$ profile, without any transverse structure (see Fig. 13). Moreover, the corresponding $1D$ profile does not correspond to the experimentally observed profiles in [11–13] shown in Fig. 9.

9. Conclusion

We propose a numerical method consisting in 'physical' splitting of the hyperbolic non-conservative equations for shear shallow water flows. Each split subsystem is hyperbolic, contains only one type of waves, and admits the energy and 'entropy' conservation laws. Moreover, such a splitting allows us to naturally define a weak solution to our system which is compatible with the positive definiteness of the Reynolds stress tensor **P**. The dissipative terms respecting the positive definiteness of **P** are further introduced. In the limit of one-dimensional flows, the roll waves solutions obtained earlier in [38,40] are recovered.

An interesting feature of the model is the formation of transverse structures at the jump toe perimeter ('fingers') from one-dimensional initial data which are harmonically perturbed in the transverse direction. The number of waves does not depend neither on the amplitude nor on the number of transverse waves in the initial perturbation. Thus, the full transition scenario is observed in the formation of roll waves: from uniform flow to one-dimensional roll waves, and, finally, to $2D$ transverse 'fingering' of roll wave profiles.

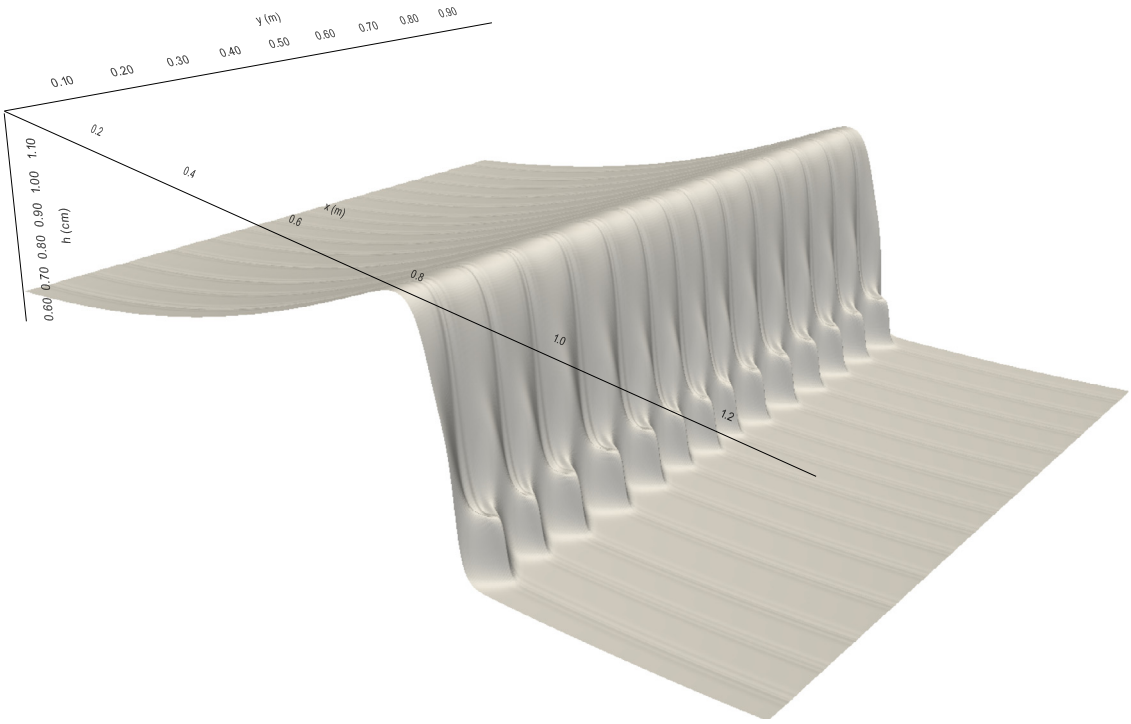

Fig. 11. Formation of transverse structures at the jump toe perimeter consisting of fourteen waves. The convergent solution is obtained for the domain 1.3 m long and 1 m wide, and shown at time instant 39 s. The Godunov method was used with 600×1200 grid cells for the parameter set mentioned above. CFL number is 0.1.

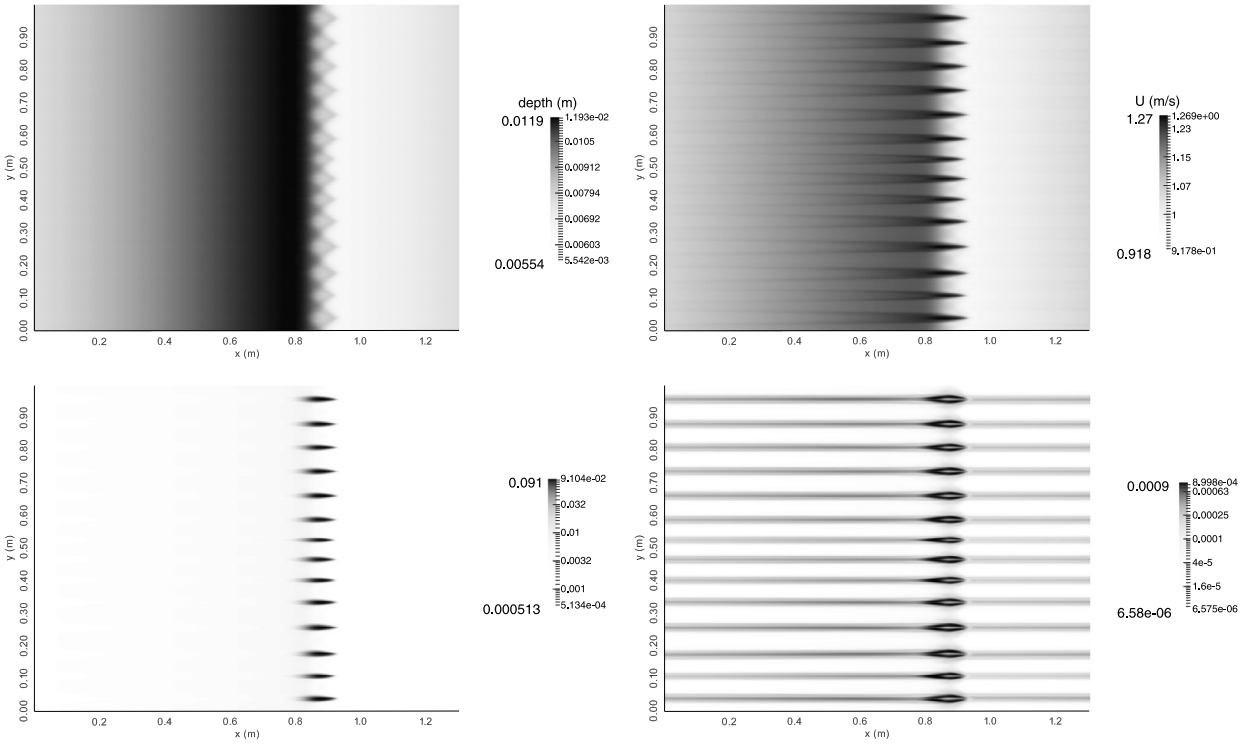

Fig. 12. Top view for the schlieren image of the fluid depth h, horizontal velocity u and normal stress components P_{11} and P_{22} are shown at the time instant 39 s. The computational domain is 1.3 m long and 1 m wide. The Godunov method was used, with 600×1200 grid cells for the parameter set mentioned above. CFL number here is 0.1. Fourteen transverse waves are observed.

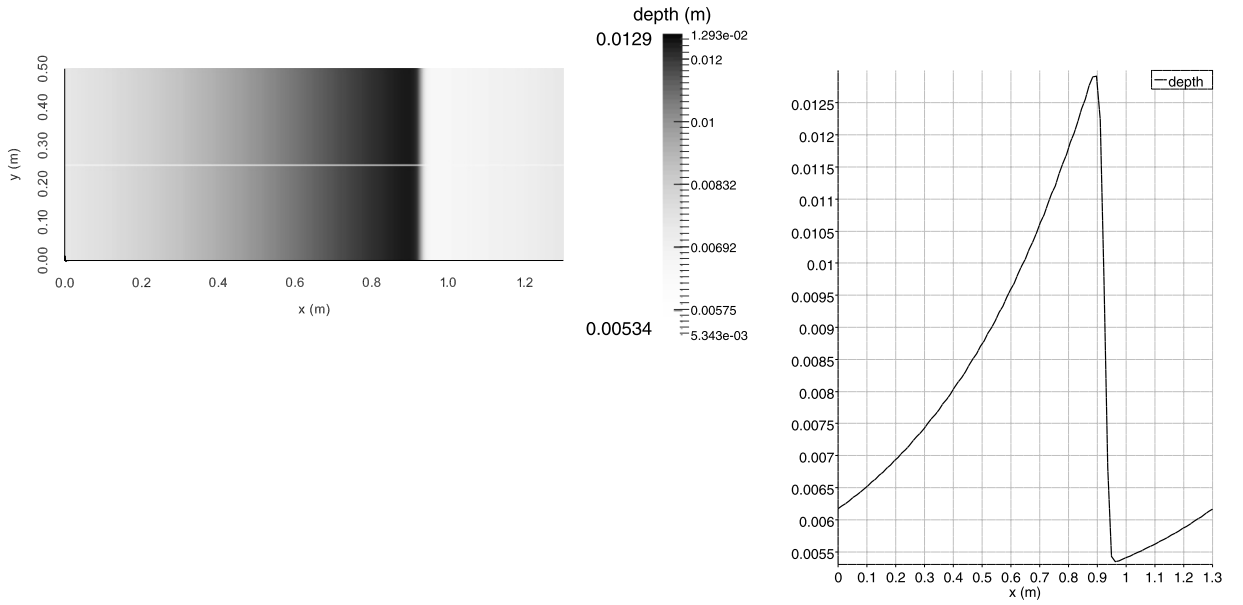

Fig. 13. Top view for the schlieren images of the fluid depth (on the left) and depth profile (on the right) with initial data (76) with $m = 1$ and $k = 4$. The new dissipation law (34) was taken. The result obtained is very surprising: transverse structures are not developed. The second fact, less surprising, is that the one-dimensional profile is not that of Brock's type.

To cover a larger domain of applications, the dispersive effects should also be included into the model. Although the corresponding mathematical models were already derived in the past (cf. [14], [41], [23]), their numerical applications are only one-dimensional. The main difficulty, as before, lies in their non-conservativity in the multi-dimensional case. We can now hope to generalize the splitting technique proposed here to the dispersive case.

The method can be extended to the general $3D$ Reynolds averaged models of barotropic flows, because the structure of the governing equations is exactly the same. The case of non-barotropic turbulent flows demands an additional modelling because both entropies, physical and 'mathematical', will increase across the shock. Thus it will be necessary to separate such an increase into two parts: the thermodynamic and turbulent ones [43]. This will be the subject of our future work.

Acknowledgement

The authors thank Boniface Nkonga for useful discussion. This work was partially supported by l'Agence Nationale de la Recherche, France (grant numbers ANR-13-BS01-0009-01, ANR-11-LABEX-0092, and ANR-11-IDEX-0001-02).

Appendix A. Conservation laws

We write down once again the governing equations for shear flows without right hand sides:

$$
\begin{aligned}
&h_t + uh_x + vh_y + hu_x + hv_y = 0, \\
&u_t + uu_x + vu_y + gh_x + \frac{1}{h}(hP_{11})_x + \frac{1}{h}(hP_{12})_y = 0, \\
&v_t + uv_x + vv_y + gh_y + \frac{1}{h}(hP_{12})_x + \frac{1}{h}(hP_{22})_y = 0, \\
&P_{11t} + uP_{11x} + vP_{11y} + 2P_{11}u_x + 2P_{12}u_y = 0, \\
&P_{12t} + uP_{12x} + vP_{12y} + P_{12}\left(u_x + v_y\right) + P_{11}v_x + P_{22}u_y = 0, \\
&P_{22t} + uP_{22x} + vP_{22y} + 2P_{12}v_x + 2P_{22}v_y = 0.
\end{aligned}
\tag{77}
$$

We are looking for conservation laws admitting by (77):

$$
\frac{\partial f}{\partial t} + \frac{\partial g_1}{\partial x} + \frac{\partial g_2}{\partial y} = 0, \tag{78}
$$

where the unknown functions f, g_1, g_2 depend on h, $\mathbf{u}$ and $\mathbf{P}$. Developing (78) one obtains:

$$
\begin{aligned}
&f_h h_t + f_u u_t + f_v v_t + f_{P_{11}} P_{11t} + f_{P_{12}} P_{12t} + f_{P_{22}} P_{22t} + g_{1h} h_x + g_{1u} u_x + g_{1v} v_x + g_{1P_{11}} P_{11x} \\
&+ g_{1P_{12}} P_{12x} + g_{1P_{22}} P_{22x} + g_{2h} h_y + g_{2u} u_y + g_{2v} v_y + g_{2P_{11}} P_{11y} + g_{2P_{12}} P_{12y} + g_{2P_{22}} P_{22y} = 0.
\end{aligned}
$$

Substituting the time derivatives of unknowns from (77) we have:

$$
\begin{aligned}
&f_h\left(-h_x u - h u_x - h_y v - h v_y\right) + f_u\left(-u u_x - v u_y - g h_x - P_{11x} - P_{12y} - \tfrac{P_{11}}{h} h_x - \tfrac{P_{12}}{h} h_y\right)\\
&+ f_v\left(-u v_x - v v_y - g h_y - P_{12x} - P_{22y} - \tfrac{P_{12}}{h} h_x - \tfrac{P_{22}}{h} h_y\right) + f_{P_{11}}\left(-u P_{11x} - v P_{11y} - 2P_{11} u_x - 2P_{12} u_y\right)\\
&+ f_{P_{12}}\left(-u P_{12x} - v P_{12y} - P_{12} u_x - P_{22} u_y - P_{11} v_x - P_{12} v_y\right) + f_{P_{22}}\left(-u P_{22x} - v P_{22y} - 2P_{12} v_x - 2P_{22} v_y\right)\\
&+ g_{1h} h_x + g_{1u} u_x + g_{1v} v_x + g_{1P_{11}} P_{11x} + g_{1P_{12}} P_{12x} + g_{1P_{22}} P_{22x}\\
&+ g_{2h} h_y + g_{2u} u_y + g_{2v} v_y + g_{2P_{11}} P_{11y} + + g_{2P_{12}} P_{12y} + g_{2P_{22}} P_{22y} = 0.
\end{aligned}
\tag{79}
$$

As the space derivatives of unknowns are independent, and (79) should be satisfied identically, we obtain the following overdetermined system of equations:

$$-u f_h - g f_u - \frac{P_{12}}{h} f_v - \frac{P_{11}}{h} f_u + g_{1h} = 0, \tag{80a}$$

$$-h f_h - u f_u - 2P_{11} f_{P_{11}} - P_{12} f_{P_{12}} + g_{1u} = 0, \tag{80b}$$

$$-u f_v - 2P_{12} f_{P_{22}} - P_{11} f_{P_{12}} + g_{1v} = 0, \tag{80c}$$

$$-v f_h - \frac{P_{12}}{h} f_u - g f_v - \frac{P_{22}}{h} f_v + g_{2h} = 0, \tag{80d}$$

$$-h f_h - v f_v - 2P_{22} f_{P_{22}} - P_{12} f_{P_{12}} + g_{2v} = 0, \tag{80e}$$

$$-v f_u - 2P_{12} f_{P_{11}} - P_{22} f_{P_{12}} + g_{2u} = 0, \tag{80f}$$

$$-f_u - u f_{P_{11}} + g_{1P_{11}} = 0, \tag{80g}$$

$$-f_v - u f_{P_{12}} + g_{1P_{12}} = 0, \tag{80h}$$

$$-u f_{P_{22}} + g_{1P_{22}} = 0, \tag{80i}$$

$$-f_u - v f_{P_{12}} + g_{2P_{12}} = 0, \tag{80j}$$

$$-f_v - v f_{P_{22}} + g_{2P_{22}} = 0, \tag{80k}$$

$$-v f_{P_{11}} + g_{2P_{11}} = 0. \tag{80l}$$

A useful remark is that there is no conservation laws with the density f depending only on $\mathbf{P}$. The remark will allow us to neglect in determining f the integration 'constants' depending only on $\mathbf{P}$. Indeed, equations (80g)–(80l) imply that in this case up to an additive constant $g_1 = uf$, $g_2 = vf$. The equations (80b), (80c), (80e) and (80f) form then a linear with respect to f overdetermined system of equations. The analysis shows that the solution is only trivial.

Eliminating the functions g_1 and g_2 from the last 6 equations of (80) we obtain:

$$
\begin{cases}
f_{uP_{11}} = 0,\\
f_{uP_{22}} = 0,\\
f_{uP_{12}} = 0,\\
f_{vP_{11}} = 0,\\
f_{vP_{12}} = 0,\\
f_{vP_{22}} = 0.
\end{cases}
\tag{81}
$$

It implies:

$$f\left(h, u, v, P_{11}, P_{12}, P_{22}\right) = f_1\left(h, u, v\right) + f_2\left(h, P_{11}, P_{12}, P_{22}\right),$$

where f_i, $i = 1, 2$, are arbitrary functions (in the following, several new arbitrary functions will appear). Eliminating the functions g_1 and g_2 from the first 6 equations of (80) we obtain:

$$h^2\left(\frac{f}{h}\right)_{hu} + \left(P_{12} f_{P_{12}} + 2P_{22} f_{P_{22}}\right)_u - \left(P_{22} f_{P_{12}} + 2P_{12} f_{P_{11}}\right)_v = 0, \tag{82a}$$

$$h^2\left(\frac{f}{h}\right)_{hv} + \left(P_{12} f_{P_{12}} + 2P_{11} f_{P_{11}}\right)_v - \left(P_{11} f_{P_{12}} + 2P_{12} f_{P_{22}}\right)_u = 0, \tag{82b}$$

$$\left(\frac{P_{12}}{h} f_u + \left(g + \frac{P_{22}}{h}\right) f_v\right)_u - \left(P_{22} f_{P_{12}} + 2P_{12} f_{P_{11}}\right)_h = 0, \tag{82c}$$

$$\left(\frac{P_{12}}{h} f_v + \left(g + \frac{P_{11}}{h}\right) f_u\right)_v - \left(P_{11} f_{P_{12}} + 2P_{12} f_{P_{22}}\right)_h = 0, \tag{82d}$$

$$\left(\frac{P_{12}}{h}f_u+\left(g+\frac{P_{22}}{h}\right)f_v\right)_v-\left(P_{12}f_{P_{12}}+2P_{22}f_{P_{22}}\right)_h-hf_{hh}=0, \tag{82e}$$

$$\left(\frac{P_{12}}{h}f_v+\left(g+\frac{P_{11}}{h}\right)f_u\right)_u-\left(P_{12}f_{P_{12}}+2P_{11}f_{P_{11}}\right)_h-hf_{hh}=0. \tag{82f}$$

In particular, (81), (82a) and (82b) imply:

$$\left(\frac{f}{h}\right)_{hu}=0,\ \left(\frac{f}{h}\right)_{hv}=0. \tag{83}$$

Then (81) and (83) imply:

$$f\left(h,u,v,P_{11},P_{12},P_{22}\right)=hc_1\left(u,v\right)+f_2\left(h,P_{11},P_{12},P_{22}\right). \tag{84}$$

Taking the difference (82c) and (82d), then (82e) and (82f), and differentiating these differences with respect to u and v, one can immediately derive that $c_1(u,v)$ is quadratic with respect to u and v:

$$c_1(u,v)=kuv+n_1u^2+n_2u+m_1v^2+m_2v,$$

where k, n_1, n_2, m_1, m_2 are constants. The general form f is then:

$$f\left(h,u,v,P_{11},P_{12},P_{22}\right)=h(kuv+n_1u^2+n_2u+m_1v^2+m_2v)+f_2\left(h,P_{11},P_{12},P_{22}\right). \tag{85}$$

The next step is thus to determine the function $f_2(h,P_{11},P_{12},P_{22})$ from the overdetermined system obtained by replacing (85) into (82c), (82d), (82e) and (82f):

$$2P_{12}n_1+\left(gh+P_{22}\right)k-\left(P_{22}f_{2P_{12}}+2P_{12}f_{2P_{11}}\right)_h=0, \tag{86a}$$

$$2P_{12}m_1+\left(gh+P_{11}\right)k-\left(P_{11}f_{2P_{12}}+2P_{12}f_{2P_{22}}\right)_h=0, \tag{86b}$$

$$P_{12}k+2\left(gh+P_{22}\right)m_1-\left(P_{12}f_{2P_{12}}+2P_{22}f_{2P_{22}}\right)_h-hf_{2hh}=0, \tag{86c}$$

$$P_{12}k+2\left(gh+P_{11}\right)n_1-\left(P_{12}f_{2P_{12}}+2P_{11}f_{2P_{11}}\right)_h-hf_{2hh}=0. \tag{86d}$$

Taking the difference of (86c) and (86d) and differentiating this difference with respect to h, one obtains:

$$P_{11}\left(f_{2hh}\right)_{P_{11}}-P_{22}\left(f_{2hh}\right)_{P_{22}}=g\left(n_1-m_1\right).$$

The general solution of this equation is:

$$f_{2hh}=\phi\left(h,P_{12},X\right)+g\left(n_1-m_1\right)\ln P_{11},\ \text{with}\ \ X=P_{11}P_{22}. \tag{87}$$

Taking now the difference of (86a) and (86b) and differentiating this difference with respect to h, one obtains:

$$\left(P_{11}-P_{22}\right)\left(f_{2hh}\right)_{P_{12}}+2P_{12}\left(\left(f_{2hh}\right)_{P_{22}}-\left(f_{2hh}\right)_{P_{11}}\right)=0 \tag{88}$$

Substituting (87) into (88) we obtain:

$$\left(P_{11}^2-X\right)\frac{\partial\phi\left(h,P_{12},X\right)}{\partial P_{12}}+2P_{12}\left(P_{11}^2-X\right)\frac{\partial\phi\left(h,P_{12},X\right)}{\partial X}-2P_{12}g\left(m_1-n_1\right)=0.$$

This is a polynomial of degree two in P_{11}. Since the identity should be valid for any P_{11}, the coefficients of the polynomial vanish. This implies: $\phi_{P_{12}}+2P_{12}\phi_X=0$ and $m_1=n_1$. Integrating two times in h, one obtains the general expression of f_2:

$$f_2=\phi_1(h,P_{11}P_{22}-P_{12}^2)+h\phi_2(\mathbf{P})+\phi_3(\mathbf{P}).$$

One can always take $\phi_3(\mathbf{P})$ vanishing because there is no conservation law with f depending only on $\mathbf{P}$. With the condition $m_1=n_1$ the difference (86c)–(86d) becomes:

$$P_{11}\phi_{2P_{11}}-P_{22}\phi_{2P_{22}}=\left(P_{11}-P_{22}\right)n_1.$$

Hence,

$$\phi_2\left(\mathbf{P}\right)=n_1\left(P_{11}+P_{22}\right)+\nu_1\left(P_{12},X\right),$$

and

$$f_2\left(h,\mathbf{P}\right)=\phi_1\left(h,P_{11}P_{22}-P_{12}^2\right)+n_1h\left(P_{11}+P_{22}\right)+h\nu_1\left(P_{12},X\right).$$

We substitute the function $f_2(h,\mathbf{P})$ into the equation (86a) and obtain:

$$(gh+P_{22})k-(P_{22}\nu_{1P_{12}}+2P_{12}P_{22}\nu_{1X})=0. \tag{89}$$

This is a linear function with respect to P_{22}. It identically vanishes if and only if:

$$k=0,\ \nu_{1P_{12}}+2P_{12}\nu_{1X}=0.$$

Hence, ν_1 is a function of only one argument $\Delta=P_{11}P_{22}-P_{12}^2$. One can insert this function into the general expression of f_2. One has now:

$$f_2(h,\mathbf{P})=\psi_1\left(h,\,P_{11}P_{22}-P_{12}^2\right)+n_1h\left(P_{11}+P_{22}\right), \tag{90}$$

with a new function ψ_1 of h and Δ. A simplified form of (86) is now:

$$2P_{12}n_1-\left(P_{22}f_{2P_{12}}+2P_{12}f_{2P_{11}}\right)_h=0, \tag{91a}$$

$$2P_{12}n_1-\left(P_{11}f_{2P_{12}}+2P_{12}f_{2P_{22}}\right)_h=0, \tag{91b}$$

$$2\left(gh+P_{22}\right)n_1-\left(P_{12}f_{2P_{12}}+2P_{22}f_{2P_{22}}\right)_h-hf_{2hh}=0, \tag{91c}$$

$$2\left(gh+P_{11}\right)n_1-\left(P_{12}f_{2P_{12}}+2P_{11}f_{2P_{11}}\right)_h-hf_{2hh}=0. \tag{91d}$$

The equations (91a), (91b) are identically satisfied if we replace expression f_2 given by (90). The equations (91c), (91d) give us the same equation:

$$2\Delta\left(\psi_{1h}\right)_\Delta+h\left(\psi_{1h}\right)_h=2ghn_1.$$

Its solution is:

$$\psi_{1h}(h,\Delta)=A\left(\frac{\Delta}{h^2}\right)+2gn_1h,$$

with an arbitrary function $A(s)$, $s=\Psi=\Delta/h^2$. Integration with respect to h gives us:

$$\psi_1(h,\Delta)=hB\left(\frac{\Delta}{h^2}\right)+n_1gh^2,$$

where $B(s)$ is an arbitrary function. The final representation of the density function f is:

$$f(h,\mathbf{u},\mathbf{P})=hB\left(\frac{P_{11}P_{22}-P_{12}^2}{h^2}\right)+n_1(gh^2+h(P_{11}+P_{22})+hu^2+hv^2)+n_2hu+m_2hv,$$

where n_1, n_2, m_2 are arbitrary constants, and B is an arbitrary function of Ψ. The conservation of mass corresponds to a particular case where $B=const$.

Appendix B. Analytical solutions

The analytical solution to (1) we present here is a generalisation of the solution with linear in space velocity profile found by Sedov [45] and Ovsyannikov [36] for the Euler equations. Thus, we are looking for the solution of the type:

$$\mathbf{u}=\mathbf{A}(t)\mathbf{x},\quad h=h(t),\quad \mathbf{P}=\mathbf{P}(t).$$

Here $\mathbf{A}(t)$ is a time dependent matrix. System (1) becomes:

$$\begin{cases}\dot h+h\mathrm{tr}(\mathbf{A})=0,\\ \dot{\mathbf{A}}+\mathbf{A}^2=\mathbf{0},\\ \dot{\mathbf{P}}+\mathbf{AP}+\mathbf{PA}^T=\mathbf{0}.\end{cases} \tag{92}$$

Here 'dot' means the time derivative. The solution $\mathbf{A}(t)$ of the second equation of (92) is given in the form:

$$\mathbf{A}=\mathbf{A}_0\left(\mathbf{I}+\mathbf{A}_0t\right)^{-1},\quad \mathbf{A}_0=const.$$

Since the corresponding matrices commute, $\mathbf{A}$ can also be written as:

$$\mathbf{A}=\left(\mathbf{I}+\mathbf{A}_0t\right)^{-1}\mathbf{A}_0.$$

Then $\mathbf{P}(t)$ verifies the equation:

$$\dot{\mathbf{P}} + \mathbf{A}_0 (\mathbf{I} + \mathbf{A}_0 t)^{-1} \mathbf{P} + \mathbf{P} \left(\mathbf{I} + \mathbf{A}_0^T t \right)^{-1} \mathbf{A}_0^T = \mathbf{0} \tag{93}$$

The solution $\mathbf{P}$ of (93) is:

$$\mathbf{P} = (\mathbf{I} + \mathbf{A}_0 t)^{-1} \mathbf{P}_0 \left(\mathbf{I} + \mathbf{A}_0^T t \right)^{-1},$$

with a constant symmetric positive definite matrix $\mathbf{P}_0 = \mathbf{P}_0^T > 0$. The solution is well defined for all $t > 0$, if the matrix $\mathbf{I} + \mathbf{A}_0 t$ is invertible for any t. This is the case, for example, of antisymmetric matrix $\mathbf{A}_0$: $\mathbf{A}_0^T = -\mathbf{A}_0$. As an example, consider the initial data:

$$\mathbf{A}_0 = \begin{pmatrix} 0 & \beta \\ -\beta & 0 \end{pmatrix}, \ \mathbf{P}_0 = \begin{pmatrix} \lambda & 0 \\ 0 & \gamma \end{pmatrix}, \ h = h_0,$$

with constants β, $\lambda > 0$, $\gamma > 0$ and $h_0 > 0$. The solution is:

$$\mathbf{A}(t) = \frac{\beta}{1 + \beta^2 t^2} \begin{pmatrix} \beta t & 1 \\ -1 & \beta t \end{pmatrix}, \ \mathbf{P} = \frac{1}{(1 + \beta^2 t^2)^2} \begin{pmatrix} \lambda + \gamma \beta^2 t^2 & (\lambda - \gamma) \beta t \\ (\lambda - \gamma) \beta t & \gamma + \lambda \beta^2 t^2 \end{pmatrix}, \ h = \frac{h_0}{1 + \beta^2 t^2}.$$

References

[1] R. Abgrall, S. Karni, Two-layer shallow water systems: a relaxation approach, SIAM J. Sci. Comput. 31 (3) (2009) 1603–1627.
[2] B. Audebert, F. Coquel, Structural stability of shock solutions of hyperbolic systems in nonconservation form via kinetic relations, in: S. Benzoni-Gavage, D. Serre (Eds.), Hyperbolic Problems: Theory, Numerics, Applications, Springer, Berlin–Heidelberg, 2008.
[3] M. Baer, J. Nunziato, A two-phase mixture theory for the deflagration-to-detonation transition (DDT) in reactive granular materials, Int. J. Multiph. Flow 12 (1986) 861–889.
[4] P.G. Baines, Topographic Effects in Stratified Flows, Cambridge Univ. Press, Cambridge, 1995.
[5] A.J.C. Barré de Saint-Venant, Théorie du movement non permanent des eaux, avec application aux crues des rivières et à l'introduction des marées dans leurs lit, C. R. Acad. Sc. Paris 73 (1871) 147–154 and 237–240.
[6] B. Barros, Conservation laws for one-dimensional shallow water models for one and two-layer flows, Math. Models Methods Appl. Sci. 16 (2006) 119–137.
[7] D.J. Benney, Some properties of long nonlinear waves, Stud. Appl. Math. 52 (1973) 45–50.
[8] C. Berthon, F. Coquel, J.-M. Hérard, M. Uhlmann, An approximate solution of the Riemann problem for a realisable second-moment turbulent closure, Shock Waves 11 (2002) 245–269.
[9] N. Besse, On the waterbag continuum, Arch. Ration. Mech. Anal. 199 (2011) 453–491.
[10] F. Bouchut, Nonlinear Stability of Finite Volume Methods for Hyperbolic Conservation Laws and Well-Balanced Schemes for Sources, Birkhäuser, Basel, 2004.
[11] R.R. Brock, Development of Roll Waves in Open Channels, PhD Thesis, Caltech, 1967.
[12] R.R. Brock, Development of roll-wave trains in open channels, J. Hydraul. Div. 95 (1969) 1401–1428.
[13] R.R. Brock, Periodic permanent roll waves, J. Hydraul. Div. 96 (1970) 2565–2580.
[14] A. Castro, D. Lannes, Fully nonlinear long-wave models in the presence of vorticity, J. Fluid Mech. 759 (2014) 642–675.
[15] F. Coquel, J.M. Hérard, K. Saleh, A positive and entropy-satisfying finite volume scheme for the Baer–Nunziato model, J. Comput. Phys. 330 (2016) 401–435.
[16] G. Dal Maso, P.G. LeFloch, F. Murat, Definition and weak stability of a non-conservative product, J. Math. Pures Appl. 74 (1995) 483–548.
[17] A.N. Dremin, I.A. Karpukhin, Method of determination of shock adiabat of the dispersed substances, J. Appl. Mech. Tech. Phys. 1 (3) (1960) 184–188 (in Russian).
[18] N. Favrie, S.L. Gavrilyuk, Diffuse interface model for compressible fluid-compressible elastic-plastic solid interaction, J. Comput. Phys. 231 (2012) 2696–2723.
[19] N. Favrie, S. Gavrilyuk, S. Ndanou, A thermodynamically compatible splitting procedure in hyperelasticity, J. Comput. Phys. 270 (2014) 300–324.
[20] S. Gavrilyuk, R. Saurel, Estimation of the turbulence energy production across a shock wave, J. Fluid Mech. 549 (2006) 131–139.
[21] S.L. Gavrilyuk, H. Gouin, Geometric evolution of the Reynolds stress tensor, Int. J. Eng. Sci. 59 (2012) 65–73.
[22] S. Gavrilyuk, Multiphase flow modelling via Hamilton's principle, in: F. dell'Isola, S.L. Gavrilyuk (Eds.), Variational Models and Methods in Solid and Fluid Mechanics, Springer, Wien, 2011.
[23] S.L. Gavrilyuk, V.Yu. Liapidevskii, A.A. Chesnokov, Spilling breakers in shallow water: applications to Favre waves and to the shoaling and breaking of solitary waves, J. Fluid Mech. 808 (2016) 441–468.
[24] S.K. Godunov, A difference method for numerical calculation of discontinuous solutions of the equations of hydrodynamics, Mat. Sb. 47 (1959) 271–306.
[25] K.A. Ivanova, S.L. Gavrilyuk, B. Nkonga, G.L. Richard, Formation and coarsening of roll-waves in shear shallow water flows down an inclined rectangular channel, Comput. Fluids 159 (2017) 189–203.
[26] A.K. Kapila, R. Menikoff, J.B. Bdzil, S.F. Son, D.S. Stewart, Two-phase modeling of deflagration-to-detonation transition in granular materials: reduced equations, Phys. Fluids 13 (10) (2001) 3002–3024.
[27] P.G. LeFloch, Hyperbolic Systems of Conservation Laws. The Theory of Classical and Nonclassical Shock Waves, Birkhäuser, Basel, 2002.
[28] X. Leng, H. Chanson, Breaking bore: physical observation of roller characteristics, Mech. Res. Commun. 65 (2015) 24–29.
[29] R.J. LeVeque, Numerical Methods for Conservation Laws, Birkhäuser, Basel, 1992.
[30] V.Yu. Liapidevskii, V.M. Teshukov, Mathematical Models of Propagation of Long Waves in an Inhomogeneous Fluid, Siberian Branch of the Russian Academy of Sciences, Novosibirsk, 2000 (in Russian).
[31] K.T. Mandli, Finite Volume Methods for the Multilayer Shallow Water Equations with Applications to Storm Surges, PhD thesis, Univ. of Washington, 2011.
[32] B. Mohammadi, O. Pironneau, Analysis of the K-Epsilon Turbulence Model, John Wiley & Sons, New York, 1994.
[33] P.J. Montgomery, T.G. Moodie, On the number of conserved quantities for the two-layer shallow water equations, Stud. Appl. Math. 106 (2001) 229–259.
[34] S. Ndanou, N. Favrie, S. Gavrilyuk, Multi-solid and multi-fluid diffuse interface model: applications to dynamic fracture and fragmentation, J. Comput. Phys. 295 (2015) 523–555.

[35] L.V. Ovsyannikov, Two-layer shallow water model, J. Appl. Mech. Tech. Phys. 20 (2) (1979) 127–135.
[36] L.V. Ovsyannikov, A new solution of the hydrodynamic equations, C. R. (Dokl.) Acad. Sci. URSS 111 (1956) 47–49 (in Russian).
[37] L.V. Ovsyannikov, Lectures on the Fundamentals of Gas Dynamics, Nauka, Moscow, 1981 (in Russian).
[38] G.L. Richard, S.L. Gavrilyuk, A new model of roll waves: comparison with Brock's experiments, J. Fluid Mech. 698 (2012) 374–405.
[39] G.L. Richard, S.L. Gavrilyuk, The classical hydraulic jump in a model of shear shallow-water flows, J. Fluid Mech. 725 (2013) 492–521.
[40] G.L. Richard, Elaboration d'un modèle d'écoulements turbulents en faible profondeur: application au ressaut hydraulique et aux trains de rouleaux, PhD thesis, Aix-Marseille Université, 2013.
[41] G.L. Richard, S.L. Gavrilyuk, Modelling turbulence generation in solitary waves on shear shallow water flows, J. Fluid Mech. 773 (2015) 49–74.
[42] R. Saurel, R. Abgrall, A multiphase Godunov method for compressible multifluid and multiphase flows, J. Comput. Phys. 150 (2001) 425–467.
[43] R. Saurel, S.L. Gavrilyuk, F. Renaud, A multiphase model with internal degrees of freedom: application to shock-bubble interaction, J. Fluid Mech. 495 (2003) 283–321.
[44] R. Saurel, O. Le Metayer, J. Massoni, S. Gavrilyuk, Shock jump relations for multiphase mixtures with stiff mechanical relaxation, Shock Waves 16 (2007) 209–232.
[45] L.I. Sedov, On the integration of the equations of one-dimensional gas motion, C. R. (Dokl.) Acad. Sci. URSS 40 (1953) 753–755 (in Russian).
[46] V.M. Teshukov, On hyperbolicity of long-wave equations, Sov. Math. Dokl. 32 (1985) 469–473.
[47] V.M. Teshukov, On Cauchy problem for long-wave equations, in: P. Neittaanmäki (Ed.), Numerical Methods for Free Boundary Problems, ISMN 92, vol. 106, Birkhäuser, Basel, 1992, pp. 331–338.
[48] V. Teshukov, G. Russo, A. Chesnokov, Analytical and numerical solutions of the shallow water equations for 2-D rotational flows, Math. Models Methods Appl. Sci. 14 (2004) 1451–1479.
[49] V.M. Teshukov, Gas dynamic analogy for vortex free-boundary flows, J. Appl. Mech. Tech. Phys. 48 (2007) 303–309.
[50] E.F. Toro, Riemann Solvers and Numerical Methods for Fluid Dynamics: A Practical Introduction, Springer, Berlin–Heidelberg, 2009.
[51] O.V. Troshkin, On wave properties of an incompressible turbulent fluid, Physica A 168 (1990) 881–899.
[52] L. Truskinovsky, Kinks versus shocks, in: R. Fosdick, E. Dunn, H. Slemrod (Eds.), Shock Induced Transitions and Phase Structures in General Media, in: IMA Vol. Math. Appl., vol. 52, Springer, New York, 1993.
[53] S.B. Pope, Turbulent Flows, Cambridge Univ. Press, Cambridge, 2005.
[54] B. Van Leer, Towards the ultimate conservative difference scheme, V. A second order sequel to Godunov's method, J. Comput. Phys. 32 (1979) 101–136.
[55] D. Wilcox, Turbulence Modeling for CFD, DCW Industries, 1998.